# Narrow band region-based active contours and surfaces for 2D and 3D segmentation

Julien Mille

*Université François Rabelais de Tours, Laboratoire Informatique (EA2101)*
*64 avenue Jean Portalis, 37200 Tours, France*

**Abstract**

We describe a narrow band region approach for deformable curves and surfaces in the perspective of 2D and 3D image segmentation. Basically, we develop a region energy involving a fixed-width band around the curve or surface. Classical region-based methods, like the Chan-Vese model, often make strong assumptions on the intensity distributions of the searched object and background. In order to be less restrictive, our energy achieves a trade-off between local features of gradient-like terms and global region features. Relying on the theory of parallel curves and surfaces, we perform a mathematical derivation to express the region energy in a curvature-based form allowing efficient computation on explicit models. We introduce two different region terms, each one being dedicated to a particular configuration of the target object. Evolution of deformable models is performed by means of energy minimization using gradient descent. We provide both explicit and implicit implementations. The explicit models are a parametric snake in 2D and a triangular mesh in 3D, whereas the implicit models are based on the level set framework, regardless of the dimension. Experiments are carried out on MRI and CT medical images, in 2D and 3D, as well as 2D color photographs.

*Key words:* Segmentation, narrow band region energy, deformable model, active contour, active surface, level sets

## 1. Introduction

Segmentation by means of deformable models has been a widely studied aspect of computer vision over the last two decades. Since their introduction by Kass et al. [1], deformable models have found many applications in image segmentation and tracking. From an initial location, which may be manually or automatically provided, these models deform according to an iterative evolution algorithm until they fit one or more structures of interest. The evolution method is usually derived from the minimization of some energy functional, including regularizing terms for geometrical smoothness and external terms relating the model to the data. They are powerful tools thanks to their ability to adapt their geometry and incorporate prior knowledge about the structure of interest.

Several implementations of these active models were developed. Explicit deformable models represent the evolving boundary as a set of interconnected control points or vertices. Among these, the original 2D parametric contour and the 3D triangular mesh [2, 3] are intuitive implementations, in which the boundary is deformed by direct modifications of vertices coordinates. The main drawback is that polygon and meshes do not modify their topology naturally, i.e. techniques for detection of topological changes must be implemented beside the evolution algorithm. Conversely, implicit implementations, based on the level set framework [4], handle the evolving boundary as the zero level of a hypersurface, defined on the same domain as the image. They are often chosen for their natural handling of topological changes and intuitive extensibility to higher dimensions. Their algorithmic complexity is a function of the image resolution, making them time-consuming. Despite the development of accelerating methods, like the narrow band technique [4] or the fast marching method [5], their computational cost remains higher than their explicit counterparts.

Deformable models, whether they are explicit or implicit, are attached to the image by means of a local edge-based energy or force. Since they consider only local boundaries, classical snakes are relatively blind, in the sense they are unable to reach boundaries if their initial location is far from them. The increasing use of region terms inspired by the Mumford-Shah functional [6, 7] has proven to overcome the limitations of uniquely gradient-based models, especially when dealing with data sets suffering from noise and lack of contrast. Indeed, many anatomical structures encountered in medical imaging lend themselves to region-based segmentation. Global statistical data computed over the entire region of interest is a well established technique to improve the behaviour of snakes. Early work, including the anticipating snake by Ronfard [8] and the active region model by Ivins and Porrill [9], introduced the use of region terms in the evolution

*Email address:* julien.mille@univ-tours.fr (Julien Mille)

of parametric snakes. The region competition method by Zhu and Yuille [10] was developed later, combining aspects of snakes and region growing techniques. Many papers have dealt with region-based approaches using the level set framework, including the Chan-Vese model [11], the deformable regions by Jehan-Besson et al. [12] and the geodesic active regions by Paragios and Deriche [13]. These implementations have the advantage of adaptive topology at the expense of computational cost. In the context of 3D segmentation, a deformable mesh endowed with a Chan-Vese region energy was presented in [14], whereas Dufour et al. [15] used an implicit active surface to perform segmentation and tracking of cells, where computations are particularly time-expensive.

Most existing region-based deformable models segment images according to statistical data computed over the entire regions, i.e. the object of interest and the background. These approaches have an underlying notion of homogeneity, in the sense that image partitions should be uniform in terms of intensity, whether prior knowledge on the distribution of pixel intensities is available [16] or not. Instead of raw pixel intensity, higher level features like texture descriptors may also be considered [17]. We now focus on the region energy of the Chan-Vese model [11]. Let $R_{\text{in}}$ be the region enclosed by deformable curve $\Gamma$, and $R_{\text{out}}$ its complement. The energy penalizes the curve splitting the image into heterogeneous regions, using intensity deviations. In addition to length and area terms, the Chan-Vese model has the following global data term:

$$\begin{aligned} E_{\text{region}}^{\text{C-V}}[\Gamma] = \lambda_{\text{in}} \iint_{R_{\text{in}}} (I(\mathbf{x}) - k_{\text{in}})^2 d\mathbf{x} \\ + \lambda_{\text{out}} \iint_{R_{\text{out}}} (I(\mathbf{x}) - k_{\text{out}})^2 d\mathbf{x} \end{aligned} \tag{1}$$

where $k_{\text{in}}$ and $k_{\text{out}}$ are intensity descriptors inside and outside the curve, respectively. By gradient descent, these descriptors are assigned to average intensity values [11]. At the end of the segmentation process, region $R_{\text{in}}$ is expected to coincide with the target object. Hence, although constraints on intensity deviations can be adjusted by tuning parameters $\lambda_{\text{in}}$ and $\lambda_{\text{out}}$, the global region term is by definition devoted to segment uniform objects and backgrounds. Let us consider the images depicted in fig. 1, in which the object of interest is the white cup. Ignoring the influence of illumination changes, case (a) is the typical configuration which the Chan-Vese model aims at, since the cup and the floor areas are nearly constant with respect to color.

Uniformity of intensity over regions is a rather strong assumption. However, strict homogeneity is not necessarily a desirable property, especially for the background. The ideal case (a) is rarely encountered in most of computer vision applications. For instance, when one wants to isolate a single structure from the rest

(a) (b) (c)

Figure 1: Different object configurations for different region energies

of the image in medical data, the background contains various anatomical structures, which differ in their overall intensities and textures. In this context, the use of local features was already addressed in the literature. For other work dealing with local statistics in region-based segmentation, the reader may refer to [18, 19, 20, 21]. For the same purpose, active contours embedded with both edge and region terms were studied in [22, 23, 24] and extended to textured region segmentation [25]. In cases (b) and (c), the background, made up of the floor and the plate, is now piecewise uniform. Case (b) depicts a particular situation where the background is uniform in a small band around the cup boundaries. We believe that many objects can be discriminated from the background according to intensity features only in the vicinity of their boundaries, which leads to the development of our first narrow band region energy. Extending the work in [26], we formulate our energy as the intensity variance over an inner and an outer band around the evolving boundary. Case (c) represents an even more general case, where the outer band around the target object is piecewise constant. Indeed, the cup is surrounded by the floor in the upper half and the plate in the bottom half. The role of our second narrow band region energy is to handle configurations in which the outer neighborhood of the target object presents several distinct areas.

In the paper, we first describe the theoretical framework of the narrow band energy. This includes mathematical derivations to yield a suitable form for the region term, i.e. a formulation enabling natural implementation. Our mathematical development is based on the theory of parallel curves and surfaces [27, 28]. We endeavour to develop a framework which is applicable both to 2D and 3D segmentation. Indeed, after describing our region terms on a planar curve, we extend them to a deformable surface model. Then, in order to allow gradient descent afterwards, we determine the variational derivatives of the region energies with respect to the curve, thanks to calculus of variations, and extend them to the surface model as well. Then, we deal with numerical implementation issues, including model structure and energy minimization. We first present the explicit implementation, which lies in a 2D polygonal contour and a 3D triangular mesh. These models are able to perform resampling, in order to overcome the lack of geometrical flexibility of traditional snakes and meshes. We also provide a level-set implementation, which

offers the advantage of a common mathematical description in 2D and 3D, in addition to the topological adaptability. Finally, experiments are carried out on medical data and natural color images. For both explicit and implicit implementations, the tests discuss the advantages of our narrow band terms over other data terms including edge energies and global region energies.

## 2. Active contour model

### *2.1. Energies*

The continuous active contour model is represented as a parameterized curve $\Gamma$ with position vector $\mathbf{c}$:

$$\begin{aligned} \Gamma : \quad & \Omega \longrightarrow \mathbb{R}^2 \\ & u \longmapsto \mathbf{c}(u) = [x(u)\ y(u)]^T \end{aligned} \tag{2}$$

where $x$ and $y$ are continuously differentiable with respect to parameter $u$. The parameter domain is normalized: $\Omega = [0, 1]$. We assume that the curve is simple, i.e. non-intersecting, and closed: $\mathbf{c}(0) = \mathbf{c}(1)$. Segmentation of an object of interest is performed by finding the curve $\Gamma$ minimizing the following energy functional:

$$E[\Gamma] = \omega E_{\text{smooth}}[\Gamma] + (1 - \omega) E_{\text{region}}[\Gamma] \tag{3}$$

where $E_{\text{smooth}}$ and $E_{\text{region}}$ are respectively the smoothness and region energies. The user-provided coefficient $\omega$ weights the significance of the smoothness term. We express the smoothness energy in terms of first-order derivative, as it appears in the original snake model by Kass et al. [1]:

$$E_{\text{smooth}}[\Gamma] = \int_{\Omega} \left\| \frac{d\mathbf{c}}{du} \right\|^2 du \tag{4}$$

The first-order regularization term usually prevents the contour to undergo large variations of its area. In our case, it is a non desirable property, since the contour will be initialized as a small shape inside a target object and inflated afterwards. Once discretized as a polygon, the contour is periodically reparameterized to keep control points practically equidistant and to allow inflation. In this context, resampling and remeshing techniques are discussed in section 5.

Curve $\Gamma$ splits the image domain $\mathcal{D}$ into an inner region $R_{\text{in}}$ and an outer region $R_{\text{out}}$, over which the homogeneity criterion is usually expressed. The narrow band principle, which has proven its efficiency in the evolution of level sets [4], is used in our approach to formulate a new region term. Instead of dealing with the entire domains delineated by the evolving curve, we only consider an inner and outer band both sides apart from the curve, as depicted in fig. 2. One may note that the bands are not limited to the snake's initial location and are updated during curve evolution.

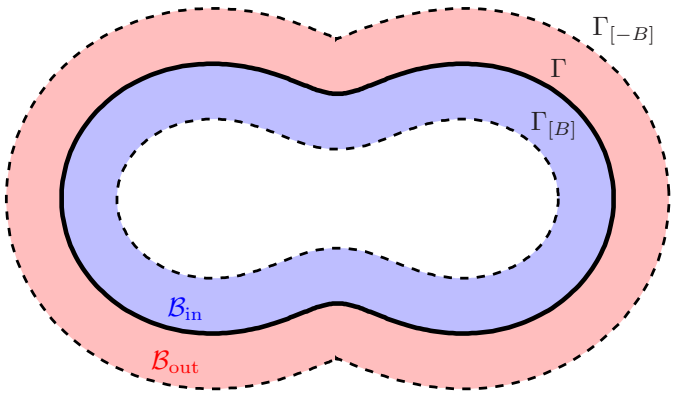


Figure 2: Inner and outer bands for narrow band region energy

Let $\mathcal{B}_{\text{in}}$ be the inner band domain and $\mathcal{B}_{\text{out}}$ the outer band domain (see fig. 2), and $B$ the band thickness, which is constant as we move along $\Gamma$. We propose two different region energies. Thus, in eq. (3), the region term will be either $E_{\text{region}_1}$ or $E_{\text{region}_2}$. To obtain $E_{\text{region}_1}$, we consider eq. (1) and we replace $R_{\text{in}}$ with $\mathcal{B}_{\text{in}}$ and $R_{\text{out}}$ with $\mathcal{B}_{\text{out}}$, which yields:

$$E_{\text{region}_1}[\Gamma] = \iint_{\mathcal{B}_{\text{in}}} (I(\mathbf{x}) - k_{\text{in}})^2 d\mathbf{x} + \iint_{\mathcal{B}_{\text{out}}} (I(\mathbf{x}) - k_{\text{out}})^2 d\mathbf{x} \tag{5}$$

Increased flexibility is achieved thanks to the narrow band principle, since it does not convey a strict homogeneity condition like classical region-based approaches. The second energy is a generalization of the first one. Its purpose is to handle cases where the background is locally homogeneous in the vicinity around the object (see fig. 1c). For now, we express it using a local outer descriptor $h_{\text{out}}$ depending on current position $\mathbf{x}$:

$$E_{\text{region}_2}[\Gamma] = \iint_{\mathcal{B}_{\text{in}}} (I(\mathbf{x}) - k_{\text{in}})^2 d\mathbf{x} + \iint_{\mathcal{B}_{\text{out}}} (I(\mathbf{x}) - h_{\text{out}}(\mathbf{x}))^2 d\mathbf{x} \tag{6}$$

In eq. (1), one may note that the Chan-Vese region term is asymmetric, as region integrals are independently weighted in order to favour minimization of intensity deviation inside or outside. However, we use symmetric terms in our approach, as it is the most common case with region-based active contours. In what follows, we show in what extent the narrow band principle allows easier implementation than classical region-based approaches.

### *2.2. Parallel curves*

The theoretical background of our narrow band framework is based on parallel curves, also known as "offset curves" [27, 28]. The curve $\Gamma_{[B]}$ is called a parallel curve of $\Gamma$ if its position vector $\mathbf{c}_{[B]}$ verifies

$$\mathbf{c}_{[B]}(u) = \mathbf{c}(u) + B\mathbf{n}(u) \tag{7}$$

where $B$ is a real constant, corresponding to the amount of translation, and $\mathbf{n}$ in the inward unit normal of $\Gamma$.

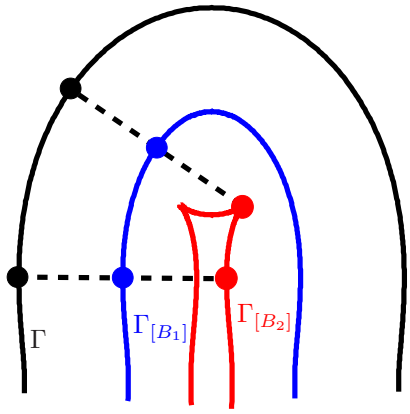


Figure 3: Main curve (black) and two parallel curves. Small translation $B_1$ yields regular curve (blue) whereas large translation $B_2$ yields a curve with singulaties (red). Corresponding points on parallel curves are linked with dashed lines.

Hereafter, we will use the index $[B]$ to denote all quantities related to the parallel curve. The definition in eq. (7) is suitable to our narrow band formulation, in the sense that bands $\mathcal{B}_{\text{in}}$ and $\mathcal{B}_{\text{out}}$ are bounded by parallel curves of $\Gamma$, respectively $\Gamma_{[B]}$ and $\Gamma_{[-B]}$. This implies that both curves are continuously differentiable and do not exhibit singularities. Fig. 3 depicts a case where width $B_2$, unlike $B_1$, is larger than the curve's radius of curvature, yielding singularities (also known as cusps). Afterwards, we refer to the eroded inner region by $R_{\text{in}[B]}$, bounded by $\Gamma_{[B]}$, and the dilated inner region by $R_{\text{in}[-B]}$ bounded by $\Gamma_{[-B]}$.

Before introducing our simplification, let us recall the notion of line integral. Given a real-valued function $f$ defined over $\mathbb{R}^2$ and a domain $D \subset \mathbb{R}^2$, we introduce the general notation $J(f, D)$ representing the integral of $f$ over domain $D$. If $D$ is a region $R$, $J(f, R)$ is an area integral whereas if $D$ is a curve $\Gamma$, $J(f, \Gamma)$ is written as a line integral:

$$J(f,\Gamma) = \int_\Omega f(\mathbf{c}(u)) \left\| \frac{d\mathbf{c}}{du} \right\| du \tag{8}$$

where the length element (or velocity)

$$\ell = \left\| \frac{d\mathbf{c}}{du} \right\| \tag{9}$$

makes $J(f, \Gamma)$ intrinsic, i.e. independent of the parameterization. This idea was first introduced in deformable models with the geodesic active contour model [29, 30, 31]. From now on, we will use indexed notations for derivatives:

$$\mathbf{c}_u = \frac{d\mathbf{c}}{du} \ , \ \mathbf{c}_{uu} = \frac{d^2\mathbf{c}}{du^2} \ ... \tag{10}$$

The curvature of $\Gamma$ is:

$$\kappa(u) = \frac{x_u y_{uu} - x_{uu} y_u}{(x_u^2 + y_u^2)^{\frac{3}{2}}} = \frac{x_u y_{uu} - x_{uu} y_u}{\ell^3}$$

An important property resulting from the definition in eq. (7) is that the velocity vector of parallel curves depends on the curvature of $\Gamma$. The velocity vector of curve $\Gamma_{[B]}$ is expressed as a function of the velocity vector of $\Gamma$, as well as its curvature and normal. Using the identity $\mathbf{n}_u = -\kappa \mathbf{c}_u$, we have:

$$\mathbf{c}_{[B]_u} = \mathbf{c}_u + B\mathbf{n}_u = (1 - B\kappa)\mathbf{c}_u \tag{11}$$

which yields, for the length element of inner parallel curve:

$$\ell_{[B]} = \left\| \mathbf{c}_{[B]_u} \right\| = \ell \, |1 - B\kappa|$$

The same development is valid for $\Gamma_{[-B]}$, replacing $B$ with $-B$. This is a known result in parallel curve theory [32, 33]. The expressions of $\ell_{[B]}$ and $\ell_{[-B]}$ suggest the smoothness condition of curves $\Gamma_{[B]}$ ans $\Gamma_{[-B]}$. Indeed, their length elements should remain strictly positive. This implies a constraint on the maximal curvature of curve $\Gamma$, i.e. the band width should not exceed the radius of curvature. We should assume that $\Gamma$ is smooth enough such that:

$$-\frac{1}{B} < \kappa(u) < \frac{1}{B}, \qquad \forall u \in \Omega \tag{12}$$

If condition 12 is well verified, curves $\Gamma_{[B]}$ and $\Gamma_{[-B]}$ are simple and regular. The impact of this assumption on numerical implementation is discussed in section 5.

### *2.3. Transformation of area integral*

In this section, we show that the domain integrals appearing in eq. (5) can be expressed in terms of $\mathbf{c}$ and $B$. This conversion is mandatory for the calculation of the variational derivative of $E_{\text{region}}$ with respect to $\mathbf{c}$. Moreover, it brings a formulation suitable for implementation on explicit models. The proof is based on Green-Riemann theorem, stating that for every region $R$, if $[P(x,y)\ Q(x,y)]^T$ is a continuously differentiable $\mathbb{R}^2 \to \mathbb{R}^2$ vector field, then:

$$\iint_R \frac{\partial Q}{\partial x} - \frac{\partial P}{\partial y} \, dxdy = \int_{\partial R} P dx + Q dy$$

In order to apply the theorem on $J(f, R)$, where $f$ is a real-valued function defined on the image domain $\mathcal{D}$, one should determine vector field $[P\ Q]$ such that

$$\frac{\partial Q}{\partial x} - \frac{\partial P}{\partial y} = k f(x,y)$$

where $k$ is a real constant. By choosing $P$ and $Q$ as follows, the previous condition is satisfied:

$$\begin{aligned} Q(x,y) &= \frac{1}{2} \int_{-\infty}^{x} f(t,y) dt \\ P(x,y) &= -\frac{1}{2} \int_{-\infty}^{y} f(x,t) dt \end{aligned} \tag{13}$$

Hereafter, we will rely on the following equation to transform region integrals:

$$J(f,R) = \int_{\partial R} P dx + Q dy \tag{14}$$

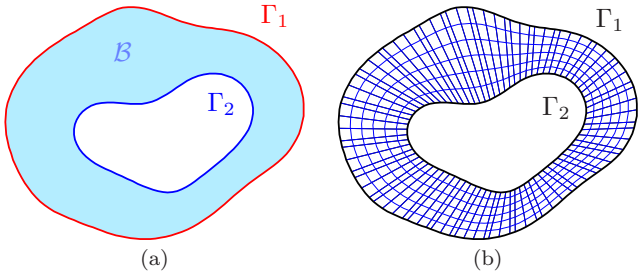


Figure 4: Region enclosed by two simple closed curves $\Gamma_1$ and $\Gamma_2$ (a) split into infinitesimal quadrilaterals (b)

Let us consider the more general case of a band $\mathcal{B}$ bounded by curves $\Gamma_1$ and $\Gamma_2$, as depicted in fig. 4a. Relying on eq. (14), the integral of $f$ over $\mathcal{B}$ is expressed using Green's theorem:

$$\begin{aligned} J(f,\mathcal{B}) &= J(f,R_1) - J(f,R_2) \\ &= \int_\Omega x_{1_u} P(\mathbf{c}_1) + y_{1_u} Q(\mathbf{c}_1) du \\ &- \int_\Omega x_{2_u} P(\mathbf{c}_2) + y_{2_u} Q(\mathbf{c}_2) du \end{aligned} \tag{15}$$

We introduce a family of curves $\{\tilde{\Gamma}(\alpha)\}_{\alpha\in[0,1]}$ interpolating from $\Gamma_1$ to $\Gamma_2$. The position vector of $\tilde{\Gamma}$ is

$$\tilde{\mathbf{c}}(\alpha,u) = (1-\alpha)\mathbf{c}_2(u) + \alpha\mathbf{c}_1(u)$$

Relying on the following equality,

$$\mathbf{c}_1 - \mathbf{c}_2 = \int_0^1 \frac{d}{d\alpha}\Big\{(1-\alpha)\mathbf{c}_2 + \alpha\mathbf{c}_1\Big\}\, d\alpha$$

and using integration by parts, we transform eq. (15) and show that $J(f,\mathcal{B})$ can be directly expressed as a function of $f$, $\mathbf{c}_1$ and $\mathbf{c}_2$ (a detailed derivation is provided in appendix A.1).

$$J(f,\mathcal{B}) = \int_\Omega\int_0^1 f(\tilde{\mathbf{c}})(\mathbf{c}_1 - \mathbf{c}_2) \times \tilde{\mathbf{c}}_u d\alpha du \tag{16}$$

This expression is intuitively understood since $(1-\alpha)\mathbf{c}_2 + \alpha\mathbf{c}_1$ sweeps all curves between $\Gamma_1$ and $\Gamma_2$ as $\alpha$ varies from 0 to 1. The cross product corresponds to the area of the infinitesimal quadrilaterals spanned by $(\mathbf{c}_1$–$\mathbf{c}_2)$ and $\tilde{\mathbf{c}}_u$, as depicted in fig. 4b. Relying on parallel curves, the mathematical definition of bands $\mathcal{B}_{\text{in}}$ allows us to express $J(f,\mathcal{B}_{\text{in}})$ in a convenient form. We apply the general result in eq. (16) on inner band $\mathcal{B}_{\text{in}}$, considering curves $\Gamma$ and $\Gamma_{[B]}$ instead of $\Gamma_1$ and $\Gamma_2$. Using a variable thickness $b$ (see appendix A.2 for more details), we finally obtain:

$$J(f,\mathcal{B}_{\text{in}}) = \int_\Omega\int_0^B f(\mathbf{c}+b\mathbf{n})\ell(1-b\kappa)dbdu \tag{17}$$

The formulation for $J(f,\mathcal{B}_{\text{out}})$ is easily obtained by replacing $b$ with $-b$ in eq. (17). This expression is especially useful when the curve is discretized as a polygonal line, as described in section 5.

### *2.4. Region energies*

Thanks to the previous result, we now express our two narrow band region energies in terms of contour, curvature and band thickness. The first narrow band region energy, which aims at minimizing the intensity deviation in the two bands, is rewritten:

$$\begin{aligned} E_{\text{region}_1}[\Gamma] &= \int_\Omega\int_0^B (I(\mathbf{c}+b\mathbf{n}) - k_{\text{in}})^2 \ell(1-b\kappa)dbdu \\ &+ \int_\Omega\int_0^B (I(\mathbf{c}-b\mathbf{n}) - k_{\text{out}})^2 \ell(1+b\kappa)dbdu \end{aligned} \tag{18}$$

For the second narrow band region energy, intensity deviation should be minimized in the outer band locally along the curve. Hence, we replace global descriptor $k_{\text{out}}$ of eq. (18) by a local counterpart, which is now a function of the position on the curve:

$$\begin{aligned} E_{\text{region}_2}[\Gamma] &= \int_\Omega\int_0^B (I(\mathbf{c}+b\mathbf{n}) - k_{\text{in}})^2 \ell(1-b\kappa)dbdu \\ &+ \int_\Omega\int_0^B (I(\mathbf{c}-b\mathbf{n}) - h_{\text{out}}(u))^2 \ell(1+b\kappa)dbdu \end{aligned} \tag{19}$$

Up to now, we have used intensity descriptors without explicitly providing their expressions. They may be considered as unknowns which will be determined during energy minimization. Their values will be determined by calculus of variations of the energies, described in section 4.

## 3. Active surface model

### *3.1. Energies*

The active contour method approach naturally extends to a three dimensional segmentation problem. In a continuous space, a deformable model is represented by a parameterized surface $\Gamma$.

$$\begin{aligned} \Gamma \;:\; & \Omega^2 \longrightarrow \mathbb{R}^3 \\ & (u,v) \longmapsto \mathbf{s}(u,v) = [x(u,v)\ y(u,v)\ z(u,v)]^T \end{aligned}$$

In all subsequent derivations, we will assume a closed surface with a parameterization homeomorphic to a torus:

$$\begin{aligned} \mathbf{s}(0,v) &= \mathbf{s}(1,v) \quad \forall v \in \Omega \\ \mathbf{s}(u,0) &= \mathbf{s}(u,1) \quad \forall u \in \Omega \end{aligned} \tag{20}$$

or a sphere:

$$\begin{aligned} \mathbf{s}(0,v) &= \mathbf{s}(1,v) \quad \forall v \in \Omega \\ \mathbf{s}(u_1,0) &= \mathbf{s}(u_2,0) \quad \forall (u_1,u_2) \in \Omega^2 \\ \mathbf{s}(u_1,1) &= \mathbf{s}(u_2,1) \quad \forall (u_1,u_2) \in \Omega^2 \end{aligned} \tag{21}$$

Note that these parameterizations are given only for mathematical transformation purpose and do not generate any constraint on the topology of the surface once this last one is discretized. Hence, they do not restrict numerical implementation. The surface is endowed with the energy

functional $E$. Replacing $\mathbf{c}$ by $\mathbf{s}$ in eq. (3), we obtain the surface energy to be minimized. The smoothness term is:

$$E_{\text{smooth}}[\Gamma] = \iint_{\Omega^2} \left\| \frac{\partial \mathbf{s}}{\partial u} \right\|^2 + \left\| \frac{\partial \mathbf{s}}{\partial v} \right\|^2 dudv \tag{22}$$

Considering now that image $I$ is a $\mathbb{R}^3 \rightarrow \mathbb{R}$ function, the narrow band region energy is a function of the volume integrals over the two bands $\mathcal{B}_{\text{in}}$ and $\mathcal{B}_{\text{out}}$:

$$\begin{aligned} E_{\text{region}_1}[\Gamma] &= \iiint_{\mathcal{B}_{\text{in}}} (I(\mathbf{x}) - k_{\text{in}})^2 d\mathbf{x} \\ &\quad + \iiint_{\mathcal{B}_{\text{out}}} (I(\mathbf{x}) - k_{\text{out}})^2 d\mathbf{x} \end{aligned} \tag{23}$$

and similarly for $E_{\text{region}_2}$. As in the two dimensional case, terms defined over bands are not computed as is. They should undergo some mathematical transformation in order to be differentiated and implemented. This is done through the framework of parallel surfaces described in the next section.

### *3.2. Parallel surfaces*

In three dimensions, regions $\mathcal{B}_{\text{in}}$ and $\mathcal{B}_{\text{out}}$ are bounded by $\Gamma$ and its parallel surfaces $\Gamma_{[B]}$ and $\Gamma_{[-B]}$, respectively. As an example, if $\Gamma$ describes a sphere, $\mathcal{B}_{\text{in}}$ and $\mathcal{B}_{\text{out}}$ may be viewed as two empty balls with thickness $B$.

$$\mathbf{s}_{[B]}(u,v) = \mathbf{s}(u,v) + B\mathbf{n}(u,v) \tag{24}$$

and similarly for $\mathbf{s}_{[-B]}$. As previous, $B$ is the constant band thickness and $\mathbf{n}(u,v)$ is the unit inward normal:

$$\mathbf{n}(u,v) = \frac{\mathbf{s}_u \times \mathbf{s}_v}{\|\mathbf{s}_u \times \mathbf{s}_v\|}$$

A surface integral of $f$ over $\Gamma$ is

$$J(f,\Gamma) = \iint_{\Omega^2} f(\mathbf{s}(u,v)) \left\| \frac{\partial \mathbf{s}}{\partial u} \times \frac{\partial \mathbf{s}}{\partial v} \right\| dudv$$

where the area element

$$a(u,v) = \left\| \frac{\partial \mathbf{s}}{\partial u} \times \frac{\partial \mathbf{s}}{\partial v} \right\| \tag{25}$$

makes the surface integral $J(f,\Gamma)$ independent of the parameterization. In accordance with our mathematical derivations in the previous section, we demonstrate how the normal vector of parallel surface can be expressed as a function of $\mathbf{s}_u \times \mathbf{s}_v$. Moreover, we show how the various surface curvatures intervene in this expression. To express surface curvature, we introduce basic elements of differential geometry [34, 33]. $E$, $F$ and $G$ are the coefficients of the first fundamental form, whereas $L$, $M$ and $N$ are the coefficients of the second fundamental form. At a given surface point $\mathbf{s}(u,v)$, we have

$$\begin{aligned} E &= \langle \mathbf{s}_u, \mathbf{s}_u \rangle \qquad F = \langle \mathbf{s}_u, \mathbf{s}_v \rangle \qquad G = \langle \mathbf{s}_v, \mathbf{s}_v \rangle \\ L &= -\langle \mathbf{n}_u, \mathbf{s}_u \rangle = \langle \mathbf{n}, \mathbf{s}_{uu} \rangle \\ M &= -\langle \mathbf{n}_u, \mathbf{s}_v \rangle = -\langle \mathbf{n}_v, \mathbf{s}_u \rangle = \langle \mathbf{n}, \mathbf{s}_{uv} \rangle \\ N &= -\langle \mathbf{n}_v, \mathbf{s}_v \rangle = \langle \mathbf{n}, \mathbf{s}_{vv} \rangle \end{aligned}$$

The gaussian curvature $\kappa_{\text{G}}$ and mean curvature $\kappa_{\text{M}}$ may be expressed in terms of coefficients of the fundamental forms:

$$\begin{aligned} \kappa_{\text{G}} &= \frac{LN - M^2}{EG - F^2} \\ \kappa_{\text{M}} &= \frac{GL - 2FM + EN}{2(EG - F^2)} \end{aligned}$$

Normal derivatives $\mathbf{n}_u$ and $\mathbf{n}_v$ are orthogonal to $\mathbf{n}$. In the tangential plane at point $\mathbf{s}(u,v)$, they can be expressed as combinations of basis vectors $\mathbf{s}_u$ and $\mathbf{s}_v$ according to the Weingarten equations [34]:

$$\begin{aligned} \mathbf{n}_u &= \frac{FM - GL}{EG - F^2}\mathbf{s}_u + \frac{FL - EM}{EG - F^2}\mathbf{s}_v \\ \mathbf{n}_v &= \frac{FN - GM}{EG - F^2}\mathbf{s}_u + \frac{FM - EN}{EG - F^2}\mathbf{s}_v \end{aligned} \tag{26}$$

which lead to the following combinations, holding mean and gaussian curvatures:

$$\begin{aligned} \mathbf{n}_u \times \mathbf{s}_v + \mathbf{s}_u \times \mathbf{n}_v &= -2\kappa_{\text{M}} \mathbf{s}_u \times \mathbf{s}_v \\ \mathbf{n}_u \times \mathbf{n}_v &= \kappa_{\text{G}} \mathbf{s}_u \times \mathbf{s}_v \end{aligned} \tag{27}$$

An important property, resulting from eq. (27), is that the normal vector of parallel surface $\Gamma_{[B]}$ is colinear to the normal vector of $\Gamma$. Its magnitude is a function of the mean and gaussian curvatures of $\Gamma$:

$$\begin{aligned} \mathbf{s}_{[B]_u} \times \mathbf{s}_{[B]_v} &= (\mathbf{s}_u + B\mathbf{n}_u) \times (\mathbf{s}_v + B\mathbf{n}_v) \\ &= (1 - 2B\kappa_{\text{M}} + B^2\kappa_{\text{G}}) \mathbf{s}_u \times \mathbf{s}_v \end{aligned} \tag{28}$$

Considering the magnitude of the previous vector, we obtain the area element of the parallel surface:

$$\begin{aligned} a_{[B]} &= \mathbf{s}_{[B]_u} \times \mathbf{s}_{[B]_v} \\ &= a \left| 1 - 2B\kappa_{\text{M}} + B^2\kappa_{\text{G}} \right| \end{aligned} \tag{29}$$

which will be useful for expressing the simplified form of the narrow band region energy described below.

### *3.3. Transformation of volume integral*

Volume integrals can be converted to surface integrals thanks to the divergence theorem, also known as Green-Ostrogradski's theorem. For every volumic region $R$, given $\mathbf{F}(\mathbf{x}) = [P(\mathbf{x})\ Q(\mathbf{x})\ R(\mathbf{x})]^T$ a continuously differentiable $\mathbb{R}^3 \rightarrow \mathbb{R}^3$ vector field, we have:

$$\iiint_R \text{div}(\mathbf{F})\ dV = \iint_{\partial R} \langle \mathbf{F}, \mathbf{N} \rangle\ dA \tag{30}$$

where $dA$ and $dV$ are the differential area and volume elements, respectively. $\mathbf{N}$ is the surface outward normal. The divergence of vector field $\mathbf{F}$ is:

$$\text{div}(\mathbf{F}) = \frac{\partial P}{\partial x} + \frac{\partial Q}{\partial y} + \frac{\partial R}{\partial z} \tag{31}$$

If the boundary $\partial R$ is parameterized by $\mathbf{s}(u,v)$, the surface integral can be written:

$$\iint_{\partial R} \langle \mathbf{F}, \mathbf{N} \rangle\, dA = -\iint_{\Omega^2} \left\langle \mathbf{F}(\mathbf{s}(u,v)), \frac{\partial \mathbf{s}}{\partial u} \times \frac{\partial \mathbf{s}}{\partial u} \right\rangle dudv \tag{32}$$

where the negative sign appears since $\mathbf{n}(u,v)$ is the unit inward normal. To convert the volume integral of $f$ into a surface integral, one should find $\mathbf{F}$ such that $\mathrm{div}(\mathbf{F}) = f$. This condition is verified by choosing $P$, $Q$ and $R$ as follows:

$$\begin{aligned} P(x,y,z) &= \frac{1}{3}\int_0^x f(t,y,z)dt \\ Q(x,y,z) &= \frac{1}{3}\int_0^y f(x,t,z)dt \\ R(x,y,z) &= \frac{1}{3}\int_0^z f(x,y,t)dt \end{aligned} \tag{33}$$

In what follows, we demonstrate how we can express the 3D region energy in terms of surface integrals. The derivation is similar in philosophy to the 2D case, since our 3D scheme is also based on curvature. As in the 2D section, we consider a general case of a volumic band $\mathcal{B}$ bounded by surfaces $\Gamma_1$ and $\Gamma_2$.

$$J(f,\mathcal{B}) = J(f,R_1) - J(f,R_2)$$

This theorem is based on a family of surfaces $\left\{\tilde{\Gamma}(\alpha)\right\}_{0\leq\alpha\leq 1}$ with position vector:

$$\tilde{\mathbf{s}}(\alpha,u,v) = (1-\alpha)\mathbf{s}_1(u,v) + \alpha\mathbf{s}_2(u,v)$$

Using the divergence theorem in eq. (32), the volume integral over the region bounded by two surfaces $\Gamma_1$ and $\Gamma_2$ can be expressed as follows (details of the proof are given in appendix A.3):

$$J(f,\mathcal{B}) = \iiint_{\Omega^2}\int_0^1 f(\tilde{\mathbf{s}})\,\langle \mathbf{s}_2-\mathbf{s}_1, \tilde{\mathbf{s}}_u\times\tilde{\mathbf{s}}_v\rangle\, d\alpha du dv \tag{34}$$

In the previous expression, the scalar triple product is the volume of the parallelepiped spanned by vectors $(\mathbf{s}_2-\mathbf{s}_1)$, $\tilde{\mathbf{s}}_u$ and $\tilde{\mathbf{s}}_v$. We apply this general result in our case, where $\Gamma_1 = \Gamma$ and $\Gamma_2 = \Gamma_{[B]}$. Given the area element of parallel surface in eq. (29), we write the final approximation of the volume integral:

$$\begin{aligned} &J(f,\mathcal{B}_{\mathrm{in}}) = \\ &\iiint_{\Omega^2}\int_0^B f(\mathbf{s}+b\mathbf{n})\,\|\mathbf{s}_u\times\mathbf{s}_v\|\,(1-2b\kappa_{\mathrm{M}}+b^2\kappa_{\mathrm{G}})dbdudv \end{aligned} \tag{35}$$

The transformation from eq. (34) to eq. (35) is detailed in appendix A.4. Again, the volume integral over outer band $\mathcal{B}_{\mathrm{out}}$ is obtained by replacing $b$ with $-b$. The first narrow band region energy is found by replacing adequates quantities in eq. (18):

$$\begin{aligned} E_{\mathrm{region}_1}[\Gamma] = &\iiint_{\Omega^2}\int_0^B a_{[b]}(I(\mathbf{s}_{[b]})-k_{\mathrm{in}})^2 dbdudv \\ &+\iiint_{\Omega^2}\int_0^B a_{[-b]}(I(\mathbf{s}_{[-b]})-k_{\mathrm{out}})^2 dbdudv \end{aligned} \tag{36}$$

where area elements $a_{[b]}$ and $a_{[-b]}$ should be expanded according to eq. (29). The explicit form of the second energy may be obtained by replacing $k_{\mathrm{out}}$ with surface-dependent local descriptor $h_{\mathrm{out}}(u,v)$.

## 4. Calculus of variations

Image segmentation is performed through numerical minimization of the energy functional using gradient descent. The negative discretized variational derivative of the energy term is usually considered for the descent direction. In this section, we express the variational derivatives of the energies, especially focusing on the region terms, for both contour and surface.

### *4.1. Active contour*

Let us consider a general energy term $E$, depending on the curve position $\mathbf{c}$ and its successive derivatives:

$$E[\Gamma] = \int_\Omega \mathcal{L}(\mathbf{c},\mathbf{c}_u,\mathbf{c}_{uu})\; du$$

The variational derivative of the energy with respect to the curve can be computed thanks to calculus of variations [1]:

$$\frac{\delta E}{\delta\Gamma} = \frac{\partial\mathcal{L}}{\partial\mathbf{c}} - \frac{d}{du}\left\{\frac{\partial\mathcal{L}}{\partial\mathbf{c}_u}\right\} + \frac{d^2}{du^2}\left\{\frac{\partial\mathcal{L}}{\partial\mathbf{c}_{uu}}\right\} \tag{37}$$

According to the Euler-Lagrange equation, if curve $\Gamma$ is a local minimizer of $E$, the previous variational derivative vanishes. Curve evolution is achieved by iterative solving of the Euler-Lagrange equation, by means of gradient descent. It is more convenient to calculate the variational derivative of each energy. From eq. (3), we have:

$$\frac{\delta E}{\delta\Gamma} = \omega\frac{\delta E_{\mathrm{smooth}}}{\delta\Gamma} + (1-\omega)\frac{\delta E_{\mathrm{region}}}{\delta\Gamma}$$

The derivative of the smoothness term is well known [1], since eq. (37) is easily applicable on $E_{\mathrm{smooth}}$:

$$\frac{\delta E_{\mathrm{smooth}}}{\delta\Gamma} = -2\frac{d^2\mathbf{c}}{du^2} \tag{38}$$

As regards the first narrow band region energy, it is more conveniently differentiated when expressed with integrals over $R_{\mathrm{in}}$ and its related regions, rather than over bands. Therefore, the inner band term is split between $R_{\mathrm{in}}$ and the eroded inner region $R_{\mathrm{in}[B]}$, whereas the outer band term is split between $R_{\mathrm{in}}$ and the dilated inner region $R_{\mathrm{in}[-B]}$, which leads to the following variational derivative:

$$\begin{aligned} &\frac{\delta E_{\mathrm{region}_1}}{\delta\Gamma} = \\ &\frac{\delta J\left((I-k_{\mathrm{in}})^2, R_{\mathrm{in}}\right)}{\delta\Gamma} - \frac{\delta J\left((I-k_{\mathrm{in}})^2, R_{\mathrm{in}[B]}\right)}{\delta\Gamma} \\ &+\frac{\delta J\left((I-k_{\mathrm{out}})^2, R_{\mathrm{in}[-B]}\right)}{\delta\Gamma} - \frac{\delta J\left((I-k_{\mathrm{out}})^2, R_{\mathrm{in}}\right)}{\delta\Gamma} \end{aligned} \tag{39}$$

In this way, region terms are transformed using Green's theorem and subsequently derived. From the appendix in [10], we have:

$$\frac{\delta J(f,R_{\mathrm{in}})}{\delta\Gamma} = -\ell f(\mathbf{c})\mathbf{n} \tag{40}$$

In appendix B, we develop the calculation of the variational derivative of the general term $J(f, R_{\text{in}[B]})$, which results in:

$$\frac{\delta J(f, R_{\text{in}[B]})}{\delta \Gamma} = -\ell(1 - B\kappa) f(\mathbf{c}_{[B]})\mathbf{n}$$

Its counterpart on the dilated region $R_{\text{in}[-B]}$ is obtained by replacing $B$ with $-B$ in eq. (67). This eventually leads to:

$$\begin{aligned} &\frac{\delta E_{\text{region}_1}}{\delta \Gamma} = \ell \big[ \\ &-(I(\mathbf{c}) - k_{\text{in}})^2 + (1 - B\kappa)(I(\mathbf{c}_{[B]}) - k_{\text{in}})^2 \\ &-(1 + B\kappa)(I(\mathbf{c}_{[-B]}) - k_{\text{out}})^2 + (I(\mathbf{c}) - k_{\text{out}})^2 \big] \, \mathbf{n} \end{aligned} \tag{41}$$

The energy should also be minimized with respect to intensity descriptors $k_{\text{in}}$ and $k_{\text{out}}$. These are found by solving

$$\frac{\partial E_{\text{region}_1}}{\partial k_{\text{in}}} = 0 \quad \text{and} \quad \frac{\partial E_{\text{region}_1}}{\partial k_{\text{out}}} = 0$$

which yield average intensities on the inner and outer bands:

$$\begin{aligned} k_{\text{in}} &= \frac{1}{|\mathcal{B}_{\text{in}}|} \int_\Omega \int_0^B I(\mathbf{c} + b\mathbf{n}) \ell (1 - b\kappa) db du \\ k_{\text{out}} &= \frac{1}{|\mathcal{B}_{\text{out}}|} \int_\Omega \int_0^B I(\mathbf{c} - b\mathbf{n}) \ell (1 + b\kappa) db du \end{aligned} \tag{42}$$

Band areas $|\mathcal{B}_{\text{in}}|$ and $|\mathcal{B}_{\text{out}}|$ are expressed by considering eq. (17) with $f(\mathbf{x}) = 1$:

$$\begin{aligned} |\mathcal{B}_{\text{in}}| &= \int_\Omega \ell \left( B - \frac{B^2}{2}\kappa \right) du \\ |\mathcal{B}_{\text{out}}| &= \int_\Omega \ell \left( B + \frac{B^2}{2}\kappa \right) du \end{aligned} \tag{43}$$

The derivative in eq. (41) holds the term $(I(\mathbf{c}) - k_{\text{out}})^2 - (I(\mathbf{c}) - k_{\text{in}})^2$, which is clearly in accordance with the region-based segmentation principle. Indeed, the sign of the above quantity depends on the likeness of the current point's intensity with respect to $k_{\text{in}}$ or $k_{\text{out}}$. If $I(\mathbf{c})$ is closer to $k_{\text{in}}$ than $k_{\text{out}}$, the contour will locally expand, as it would be the case with a region growing approach. Moreover, one may note that this term is also found in the Chan-Vese region-based method. The derivative holds additional curvature-dependent terms which are addressed in section 5.

We now deal with the second region energy. From eq. (41), we extrapolate a consistent variational derivative of the second narrow band region term. We obtain:

$$\begin{aligned} &\frac{\delta E_{\text{region}_2}}{\delta \Gamma} \approx \ell \big[ \\ &-(I(\mathbf{c}) - k_{\text{in}})^2 + (1 - B\kappa)(I(\mathbf{c}_{[B]}) - k_{\text{in}})^2 \\ &-(1 + B\kappa)(I(\mathbf{c}_{[-B]}) - h_{\text{out}})^2 + (I(\mathbf{c}) - h_{\text{out}})^2 \big] \, \mathbf{n} \end{aligned} \tag{44}$$

The local outer descriptor function $h_{\text{out}}$ is determined by solving another Euler-Lagrange equation:

$$\frac{\delta E_{\text{region}_2}}{\delta h_{\text{out}}} = 0$$

which yields the average weighted intensity along the outward normal line of length $B$, at a given contour point:

$$h_{\text{out}}(u) = \frac{\displaystyle\int_0^B \ell(1 + b\kappa) I(\mathbf{c} - b\mathbf{n}) db}{\displaystyle\int_0^B \ell(1 + b\kappa) db}$$

According to the previous definition of $h_{\text{out}}$, we assume that piecewise constancy over the outer band is verified if intensity is uniform along finite length lines in the direction normal to the object boundary. For a given point on the contour, the length element is constant and may be omitted, which reduces the mean intensity to:

$$h_{\text{out}}(u) = \frac{2}{B(2 + B\kappa)} \int_0^B (1 + b\kappa) I(\mathbf{c} - b\mathbf{n}) db \tag{45}$$

*4.2. Extension to the surface*

The general energy term depending on surface position as well as its $u$ and $v$-derivatives,

$$E[\Gamma] = \iint_{\Omega^2} \mathcal{L}(\mathbf{s}, \mathbf{s}_u, \mathbf{s}_v, \mathbf{s}_{uu}, \mathbf{s}_{uv}, \mathbf{s}_{vv}) \; du dv$$

has the following variational derivative [35]:

$$\begin{aligned} \frac{\delta E}{\delta \Gamma} &= \frac{\partial \mathcal{L}}{\partial \mathbf{s}} - \frac{d}{du}\left\{\frac{\partial \mathcal{L}}{\partial \mathbf{s}_u}\right\} - \frac{d}{dv}\left\{\frac{\partial \mathcal{L}}{\partial \mathbf{s}_v}\right\} \\ &+ \frac{d^2}{du^2}\left\{\frac{\partial \mathcal{L}}{\partial \mathbf{s}_{uu}}\right\} + \frac{d^2}{dudv}\left\{\frac{\partial \mathcal{L}}{\partial \mathbf{s}_{uv}}\right\} + \frac{d^2}{dv^2}\left\{\frac{\partial \mathcal{L}}{\partial \mathbf{s}_{vv}}\right\} \end{aligned}$$

The variation of the smoothness term is straightforward to calculate and is a function of the laplacian:

$$\frac{\delta E_{\text{smooth}}}{\delta \Gamma} = -2\left(\frac{\partial^2 \mathbf{s}}{\partial u^2} + \frac{\partial^2 \mathbf{s}}{\partial v^2}\right) \tag{46}$$

As in the 2D case, it is practical to differentiate the region term when formulated in terms of integrals over $R_{\text{in}}$, $R_{\text{in}[B]}$ and $R_{\text{in}[-B]}$. Hence, a similar derivation as in eq. (39) is performed. A detailed calculation of the variational derivative of a general term $J(f, R_{\text{in}})$ may be found in the appendix of [36]. It gives:

$$\frac{\delta J(f, R_{\text{in}})}{\delta \Gamma} = -a f(\mathbf{s})\mathbf{n}$$

The variation of the term expressed on the eroded inner region is extended from appendix B. In particular, the final result of eq. (67) gives:

$$\frac{\delta J(f, R_{\text{in}[B]})}{\delta \Gamma} = -a(1 - 2B\kappa_{\text{M}} + B\kappa_{\text{G}}) f(\mathbf{s}_{[B]})\mathbf{n}$$

and similarly on the dilated inner region. Replacing the curvature-dependent terms of eq. (41) and (44), this eventually leads to:

$$\begin{aligned}\frac{\delta E_{\text{region}_1}}{\delta \Gamma} &= a\left[-(I(\mathbf{s})-k_{\text{in}})^2+(I(\mathbf{s})-k_{\text{out}})^2\right.\\ &+(1-2B\kappa_{\text{M}}+B^2\kappa_{\text{G}})(I(\mathbf{s}_{[B]})-k_{\text{in}})^2\\ &\left.-(1+2B\kappa_{\text{M}}+B^2\kappa_{\text{G}})(I(\mathbf{s}_{[-B]})-k_{\text{out}})^2\right]\mathbf{n}\end{aligned} \tag{47}$$

Minimizing $E_{\text{region}_1}$ with respect to intensity descriptors $k_{\text{in}}$ and $k_{\text{out}}$, we end up with average intensities:

$$\begin{aligned}k_{\text{in}} &= \frac{1}{|\mathcal{B}_{\text{in}}|}\iiint_{\Omega^2\,0}^{\quad B} a_{[b]}I(\mathbf{s}_{[b]})\;dbdudv\\ k_{\text{out}} &= \frac{1}{|\mathcal{B}_{\text{out}}|}\iiint_{\Omega^2\,0}^{\quad B} a_{[-b]}I(\mathbf{s}_{[-b]})\;dbdudv\end{aligned}$$

The derivative of $E_{\text{region}_2}$ may be obtained from eq. (47), replacing $k_{\text{out}}$ with local descriptor $h_{\text{out}}(u,v)$. As in the 2D case, minimizing $E_{\text{region}_2}$ with respect to $h_{\text{out}}$, we obtain the average intensity along outer normal line segment at surface point $^{\mathbf{s}}(u,v)$:

$$\begin{aligned}&h_{\text{out}}(u,v)=\\ &\frac{3}{3B(1+B)+B^3}\int_0^B I(\mathbf{s}_{[-b]})(1+2b\kappa_{\text{M}}+b^2\kappa_{\text{G}})db\end{aligned} \tag{48}$$

Once the first variations of the smoothness and region terms are known, we are able to perform gradient descent of the discretized energy over explicit implementations of the curve and surface.

## 5. Implementation on explicit models

### *5.1. Polygon and mesh*

To describe the discrete forms of active 2D contour and 3D surface models simultaneously, we introduce a general framework. The contour is a discrete closed curve, whereas the surface model is a triangular mesh built by subdividing an icosahedron [37]. The models have a constant global topology, their initial shape being circular and spherical, respectively. Both are made up of a set of $n$ vertices, denoted $\mathbf{p}_i = [x_i\ y_i]^T$ in 2D and $\mathbf{p}_i = [x_i\ y_i\ z_i]^T$ in 3D. Each vertex $\mathbf{p}_i$ has a set of neighboring vertices, denoted $\mathcal{N}_i$. In the 2D contour, index $i$ is the discrete equivalent of the curve parameter, hence $\mathcal{N}_i = \{i-1, i+1\}$. For the mesh, $\mathcal{N}_i$ is sorted in such a way that the $k^{th}$ and $(k+1)^{th}$ neighbors of $\mathbf{p}_i$ are also neighbors between them. While the computation of tangent and normal vectors is straightforward on the polygon, computing normals on the mesh needs some explanation. The normal of vertex $\mathbf{p}_i$ is the mean computed over the normals of the neighboring triangles [3]. The normal $\mathbf{n}_t$ of a given triangle is the normalized cross product between two of its edges.

$$\mathbf{n}_t = \frac{(\mathbf{p}_{t_2}-\mathbf{p}_{t_1})\times(\mathbf{p}_{t_3}-\mathbf{p}_{t_1})}{\|(\mathbf{p}_{t_2}-\mathbf{p}_{t_1})\times(\mathbf{p}_{t_3}-\mathbf{p}_{t_1})\|} \tag{49}$$

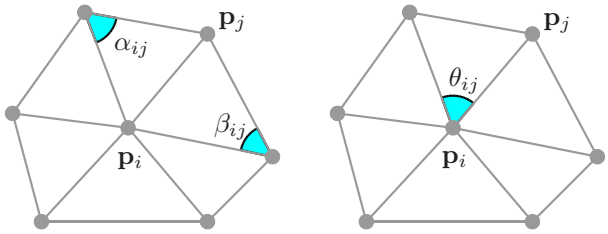


Figure 5: Angles in the neighborhood of $\mathbf{p}_i$ for discrete mean and gaussian curvature estimation

where $\mathbf{p}_{t_k}, k = 1,2,3$ are the vertices of triangle $t$. In a given triangle, vertex indices should be sorted so that the normal vector points towards the inside of the surface. Since the iterative evolution algorithm described below modifies vertex coordinates, all normals should be updated after each iteration (when all vertices have been moved). For the contour, the discretized length element $\ell$ associated to $\mathbf{p}_i$ is

$$\ell_i = \frac{\|\mathbf{p}_i-\mathbf{p}_{i-1}\|+\|\mathbf{p}_i-\mathbf{p}_{i+1}\|}{2}$$

For the mesh, to compute the area element associated to $\mathbf{p}_i$, we use the sum of areas of its neighboring triangles:

$$\mathcal{A}_i = \sum_{k=1}^{|\mathcal{N}_i|}\frac{\left\|(\mathbf{p}_i-\mathbf{p}_{\mathcal{N}_i[k]})\times(\mathbf{p}_i-\mathbf{p}_{\mathcal{N}_i[k+1]})\right\|}{2}$$

The area element is simply $a_i = \mathcal{A}_i/3$. The sum of area elements equal to the sum of triangle areas, which is itself the total mesh area. To estimate the mean and gaussian curvatures, we use the discrete operators described in [38] and [39].

$$\begin{aligned}\kappa_{\text{M}i} &= \frac{1}{4\mathcal{A}_i}\left\|\sum_{j\in\mathcal{N}_i}(\cot\alpha_{ij}+\cot\beta_{ij})(\mathbf{p}_i-\mathbf{p}_j)\right\|\\ \kappa_{\text{G}i} &= \frac{1}{\mathcal{A}_i}\left(2\pi-\sum_{j\in\mathcal{N}_i}\theta_{ij}\right)\end{aligned}$$

where $\alpha_{ij}$, $\beta_{ij}$ and $\theta_{ij}$ are the angles formed by $\mathbf{p}_i$, $\mathbf{p}_j$ and their common neighboring vertices, as shown in fig. 5.

### *5.2. Reparameterization*

To maintain a stable vertex distribution along the 2D contour (or 3D surface), adaptive resampling (or remeshing) is performed [3]. The contour is allowed to add or delete vertices to keep the distance between neighboring vertices homogeneous. It insures that every couple of neighbors $(\mathbf{p}_i, \mathbf{p}_j)$ satisfies the constraint:

$$w \le \|\mathbf{p}_i-\mathbf{p}_j\| \le 2w \tag{50}$$

where $w$ is the sampling between consecutive vertices. Resampling the 2D contour is simple: when the distance

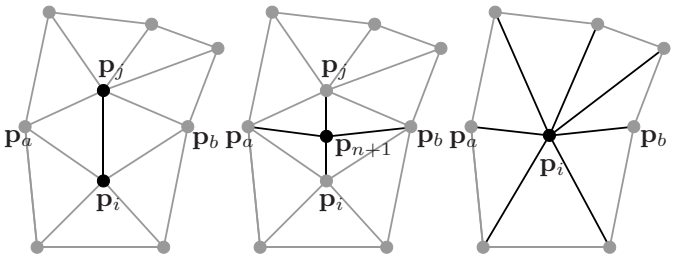


Figure 6: Remeshing operations on the triangular mesh: vertex inserting (middle) and deleting (left)

between $\|\mathbf{p}_i - \mathbf{p}_{i+1}\|$ exceeds $2w$, the line segment is split by creating a new vertex at coordinates $(\mathbf{p}_i + \mathbf{p}_{i+1})/2$. When $\|\mathbf{p}_i - \mathbf{p}_{i+1}\|$ gets below $w$, vertex $\mathbf{p}_{i+1}$ is deleted and $\mathbf{p}_i$ is connected to $\mathbf{p}_{i+2}$.

Active surface remeshing is described in [3] and [14]. While resampling the 2D contour is rather straightforward, remeshing the 3D active surface is carefully performed. Adding or deleting vertices modifies local topology, thus topological constraints should be verified. Let us consider the couple of neighbors $(\mathbf{p}_i,\mathbf{p}_j)$. To perform vertex adding or deleting, $\mathbf{p}_i$ and $\mathbf{p}_j$ should share exactly two common neighbors, denoted $\mathbf{p}_a$ and $\mathbf{p}_b$. When $\|\mathbf{p}_i - \mathbf{p}_j\| > 2w$, a new vertex is created at the middle of line segment $\mathbf{p}_i\mathbf{p}_j$ and connected to $\mathbf{p}_a$ and $\mathbf{p}_b$ (see middle part of fig. 6). When $\|\mathbf{p}_i - \mathbf{p}_j\| < w$, $\mathbf{p}_j$ is deleted and $\mathbf{p}_i$ is translated to the middle location (see right part of fig. 6). Vertex merging prevents neighboring vertices from getting too close, which might result in vertex overlapping and intersections between triangles. Adding vertices allows the contour and surface to inflate significantly while keeping a sufficient vertex density.

### *5.3. Energy minimization*

We give the discrete forms of quantities used in the region energies. Over $\mathcal{B}_{\text{in}}$, area integrals are computed according to the following template formula, which is a discrete implementation of eq. (17):

$$J(f,\mathcal{B}_{\text{in}}) \approx \sum_{i=1}^{n}\sum_{b=0}^{B-1} f(\mathbf{p}_i + b\mathbf{n}_i)\ell_i(1-b\kappa_i) \tag{51}$$

where $\ell_i$, $\mathbf{n}_i$ and $\kappa_i$ are the discretized length element, normal and curvature at vertex $\mathbf{p}_i$, using finite differences. A similar computation is performed over the outer band, in which $b$ varies from $-B$ to $-1$. There are two complementary techniques to address the regularity condition in eq. (12). The first one is to prevent each vertex from making a sharp angle with its neighbors, so that its curvature $\kappa_i$ is well bounded. Moreover, the case of a negative length element can be handled. Hence, in eq. (51), $\ell_i(1-b\kappa_i)$ is actually computed as $\max(0,\ell_i(1-b\kappa_i))$ and similarly on the outer band. Vertex coordinates are iteratively modified using gradient descent of eq. (3) with time step $\Delta t$:

$$\mathbf{p}_i^{(t+1)} = \mathbf{p}_i^{(t)} + \Delta t\mathbf{f}(\mathbf{p}_i) \tag{52}$$

where $\mathbf{f}(\mathbf{p}_i)$ is the force vector, expressed in terms of the discretization of the energy derivative at a given vertex $\mathbf{p}_i$:

$$\begin{aligned}\mathbf{f}(\mathbf{p}_i) &= -\frac{\delta E}{\delta\Gamma}\bigg|_{\mathbf{c}=\mathbf{p}_i} \\ &= \omega\mathbf{f}_{\text{smooth}}(\mathbf{p}_i) + (1-\omega)\mathbf{f}_{\text{region}}(\mathbf{p}_i)\end{aligned}$$

We first consider the region force $\mathbf{f}_{\text{region}}$ (the smoothness force is studied in the next section). To compute band areas and means on the polygonal contour, we apply the discretization templates in eq. (51) on expressions of areas in eq. (43) and intensity means in eq. (42). Similarly, quantities in the 3D region energy in eq. (36) are implemented. For the first narrow band region energy, the corresponding force on the contour is:

$$\mathbf{f}_{\text{region}_1}(\mathbf{p}_i) = \left[(I(\mathbf{p}_i)-k_{\text{in}})^2 - (I(\mathbf{p}_i)-k_{\text{out}})^2\right]\mathbf{n}_i \tag{53}$$

In addition to the squared differences between $I(\mathbf{c})$ and the average band intensities, the variational derivative in eq. (41) also contains curvature-based terms depending on the intensity at points $\mathbf{c}_{[B]}$ and $\mathbf{c}_{[-B]}$. Actually, these terms turn out to go against the region growing or shrinking principle, as they oppose the other terms depending on $I(\mathbf{c})$. As stated in [40], the usual energy gradient may not be consistently the best direction to take, which justifies our choice to remove side effect terms. Moreover, by doing so, we keep the same evolution principle as the Chan-Vese region term. In a similar way, the force resulting from the second narrow band region energy is:

$$\mathbf{f}_{\text{region}_2}(\mathbf{p}_i) = \left[(I(\mathbf{p}_i)-k_{\text{in}})^2 - (I(\mathbf{p}_i)-\mu_{\text{NL}}(\mathbf{p}_i))^2\right]\mathbf{n}_i \tag{54}$$

with

$$\mu_{\text{NL}}(\mathbf{p}_i) = B\left(1+\frac{\kappa_i(B+1)}{2}\right)\sum_{b=1}^{b=B}(1+b\kappa_i)I(\mathbf{p}_i - b\mathbf{n}_i)$$

### *5.4. Gaussian filtering*

Minimizing the regularization term boils down to apply laplacian smoothing of the contour - see eqs. (38) and (46) - which is formalized by the following PDE:

$$\frac{\partial\mathbf{c}}{\partial t} = \alpha\frac{\partial^2\mathbf{c}}{\partial u^2}$$

where $\alpha \in [0,1/2]$. When discretized, laplacian smoothing only intervenes in the direct neighborhood of vertices and is consequently limited in space. However, highly noise-corrupted data require very strong regularity constraint on the contour. Should the regularization be insufficient, the contour is exposed to unstable behaviour. Hence, to achieve more diffuse regularization, the contour is convolved with a gaussian kernel of zero mean and standard deviation $\sigma$. Regularization often comes with curve shrinkage, as studied in [41]. To avoid this unwanted effect, we

use the two-pass method of Taubin [42]. This consists in performing the gaussian smoothing twice, firstly with a positive weight and secondly with a negative one. The force, resulting from the first pass, applied on a given vertex is

$$\mathbf{f}_{\text{smooth}}(\mathbf{p}_i) = \left( \frac{1}{\sigma\sqrt{2\pi}} \sum_{k=-\eta}^{k=\eta} \exp\left(-\frac{k^2}{2\sigma^2}\right) \mathbf{p}_{i+k} \right) - \mathbf{p}_i \tag{55}$$

where $\eta$ is the rank of neighborhood. One usually admits that the value of the gaussian distribution is nearly zero beyond $3\sigma$, we choose $\eta = 3\sigma$. This force is used instead of a discretization of the variational derivative in eq. (38). A similar smoothing is performed on the deformable mesh when working with 3D data. In eq. (55), the $k^{th}$ neighbors of $\mathbf{p}_i$ should then be replaced with successive rings of neighbors - the first one being $\mathcal{N}_i$ - around $\mathbf{p}_i$. The choice of standard deviation $\sigma$ has a substantial impact on the final segmentation result and is discussed in section 7.

### *5.5. Bias force*

In a particular case, the formulation of $\mathbf{f}_{\text{region}}$ presents a shortcoming. Indeed, the magnitude of $\mathbf{f}_{\text{region}}$ is low when $k_{\text{in}}$ and $k_{\text{out}}$ are similar, since in eq. (53), the term $(I(\mathbf{p}_i)-k_{\text{out}})^2 - (I(\mathbf{p}_i)-k_{\text{in}})^2$ tends to 0. This situation arise when the contour, including the bands, is initialized inside a uniform area. However, we expect the contour to grow if the intensity at the current vertex matches the inner band features, whatever the value of $k_{\text{out}}$. Thus, we introduce a bias $\mathbf{f}_{\text{bias}}$ expanding the boundary if $I(\mathbf{p}_i)$ is near $k_{\text{in}}$ :

$$\mathbf{f}_{\text{bias}}(\mathbf{p}_i) = -\left(1 - (I(\mathbf{p}_i) - k_{\text{in}})^2\right) \mathbf{n}_i$$

This bias acts like the balloon force described in [35]. Its influence should decrease as $k_{\text{in}}$ gets far from $k_{\text{out}}$. To do so, we weight $\mathbf{f}_{\text{bias}}$ with a negative exponential-like coefficient $\gamma$.

$$\begin{aligned} \gamma &= \frac{1 - (k_{\text{in}} - k_{\text{out}})^2}{1 + \rho(k_{\text{in}} - k_{\text{out}})^2} \\ \mathbf{f}_{\text{region+bias}}(\mathbf{p}_i) &= \gamma \mathbf{f}_{\text{bias}}(\mathbf{p}_i) + (1-\gamma)\mathbf{f}_{\text{region}}(\mathbf{p}_i) \end{aligned} \tag{56}$$

where $\rho$ should be high enough to ensure a quickly decreasing slope (any value above 50 turns out to be suitable). Hence, $\mathbf{f}_{\text{bias}}$ is predominant when mean intensities are close. Its influence decreases to the advantage of $\mathbf{f}_{\text{region}}$ as inner and outer mean intensities become significantly different. One may note that the bias force is also applied when using the second region force in eq. (54). Consequently, our region terms maintain the same ability to grow or retract than classical region-based active contours. The region bias guarantees the contour has a similar capture range as other region-based models.

### *5.6. Implementation of Green's and divergence theorems*

Our experiments, described in section 7, include a comparison between segmentation results obtained with our narrow band region terms and the ones obtained with the Chan-Vese region energy in eq. (1). The implementation of the latter on the explicit polygon and mesh raises the difficulty of computing region integrals. The direct solution consists in using region filling algorithms to determine inner pixels, as in [9] and [14], which would be computationally expensive if performed after each deformation step. Another solution, which we chose, is based on an discretization of Green-Riemann and Green-Ostrogradski theorems in 2D and 3D, respectively.

In the 2D case, we consider Green's theorem as stated in eqs. (13) and (14). For instance, a brute-force implementation of the integral $J(I, R_{\text{in}})$ on the polygon would yield:

$$\begin{aligned} J(I, R_{\text{in}}) \approx \frac{1}{2} \sum_{i=1}^{n} \Bigg\{ & \frac{y_{i+1} - y_{i-1}}{2} \sum_{k=0}^{x_i} I(k, y_i) \\ & - \frac{x_{i+1} - x_{i-1}}{2} \sum_{l=0}^{y_i} I(x_i, l) \Bigg\} \end{aligned}$$

Computing this term in this way may be time-consuming, since intensities should be summed horizontally and vertically at each vertex position. Nevertheless, it is possible to compute and store the summed intensities only once, before polygon deformation is performed. This reduces the algorithmic complexity to $O(n)$, whereas narrow band region energies induce a $O(nB)$ complexity. Note that the additonal memory cost imputed to the 2D arrays, storing summed intensities in the $x$ and $y$ directions for each pixel, is insignificant.

On the other hand, for volumetric images, the extra memory burden caused by a similar implementation of the divergence theorem would be problematic. In this case, in addition to the initial image, we store a unique 3D array $S$ holding summed intensities in the $x$, $y$ and $z$ dimensions. Its corresponding continuous expression is:

$$S(x, y, z) = \int_{-\infty}^{z} \int_{-\infty}^{y} \int_{-\infty}^{x} I(x', y', z') dx' dy' dz'$$

which is actually computed according to the following recursive scheme:

$$\begin{aligned} S(x, y, z) = \; & S(x-1, y, z) + S(x, y-1, z) \\ & + S(x, y, z-1) - S(x-1, y-1, z) \\ & - S(x-1, y, z-1) - S(x, y-1, z-1) \\ & + S(x-1, y-1, z-1) + I(x, y, z) \end{aligned}$$

As in 2D, $S$ needs to be computed only once at the beginning of the segmentation process. Then, during surface

evolution, image primitives $P$, $Q$ and $R$ are determined by finite differences. We provide the details for $P$:

$$\begin{aligned} P(x,y,z) &= \frac{1}{3}\frac{\partial^2 S}{\partial y \partial z} \\ &\approx \frac{1}{3}\left(S(x,y,z) - S(x,y{-}1,z)\right. \\ &\quad \left. -S(x,y,z{-}1) + S(x,y{-}1,z{-}1)\right) \end{aligned}$$

For an implementation of the divergence theorem in the context of 3D segmentation, the reader may refer to [43].

## 6. Level set implementation

We provide an implicit implementation of our narrow band energies as well. In addition to topological flexibility, the level set formulation presents the advantage of a common formulation for both 2D and 3D models. We consider the level set function $\psi : \mathbb{R}^d \to \mathbb{R}$, where $d$ is the image dimension. The contour or surface is the zero level set of $\psi$. We define the region enclosed by the contour or surface by $R_{\text{in}} = \{\mathbf{x} | \psi(\mathbf{x}) \leq 0\}$. Instead of forces applied on vertices, we now deal with speeds applied to function samples. Function $\psi$ deforms according to the evolution equation:

$$\frac{\partial \psi}{\partial t} = F(\mathbf{x}) \left\| \nabla \psi(\mathbf{x}) \right\| \ \forall \mathbf{x} \in \mathbb{R}^d \tag{57}$$

where speed function $F$ is to some extent the level set-equivalent of the explicit energy in eq. (3), i.e. a weighted sum of smoothness and region terms:

$$F(\mathbf{x}) = \omega F_{\text{smooth}}(\mathbf{x}) + (1-\omega) F_{\text{region}}(\mathbf{x})$$

In the level set framework, regularization is usually performed with a curvature-dependent term. With this technique, for the same reasons as explained in section 5.4, the effect is limited to the direct neighborhood of pixels. In order to achieve a regularization as diffuse as in eq. (55), we replace the usual curvature term with a gaussian convolution, as in [44]:

$$F_{\text{smooth}}(\mathbf{x}) = \left( \frac{1}{\sigma\sqrt{2\pi}} \sum_{\mathbf{x}' \in \mathcal{W}_{3\sigma}(\mathbf{x})} \exp\left( -\frac{\|\mathbf{x}'-\mathbf{x}\|^2}{2\sigma^2} \right) \psi(\mathbf{x}') \right) - \psi(\mathbf{x})$$

where $\mathcal{W}$ is a circular window of a given radius around $\mathbf{x}$:

$$\mathcal{W}_\eta(\mathbf{x}) = \{\mathbf{x}' | \, \|\mathbf{x}'-\mathbf{x}\| \leq \eta\}$$

Parameters $\omega$ and $\sigma$ play the same role as in the explicit implementation described in section 5. Areas, volumes and average intensities upon inner and outer bands are easily computed on the level set implementation, since a circular window of radius $B$ may be considered around each pixel located on the front.

$$\begin{aligned} \mathcal{B}_{\text{in}} &= \{\mathbf{x} | \psi(\mathbf{x}) \leq 0 \text{ and } \exists \mathbf{x}' \in \mathcal{W}_B(\mathbf{x}) \text{ s.t. } \psi(\mathbf{x}') = 0\} \\ \mathcal{B}_{\text{out}} &= \{\mathbf{x} | \psi(\mathbf{x}) \geq 0 \text{ and } \exists \mathbf{x}' \in \mathcal{W}_B(\mathbf{x}) \text{ s.t. } \psi(\mathbf{x}') = 0\} \end{aligned}$$

If it is assumed that $\psi$ remains a signed euclidean distance function, the narrow band region energy may be written as:

$$\begin{aligned} E_{\text{region}_1}[\psi] = & \iint_{\mathcal{D}} H(\psi(\mathbf{x})+B)(1-H(\psi(\mathbf{x})))(I(\mathbf{x})-k_{\text{in}})^2 d\mathbf{x} \\ + & \iint_{\mathcal{D}} H(\psi(\mathbf{x}))(1-H(\psi(\mathbf{x})-B))(I(\mathbf{x})-k_{\text{out}})^2 d\mathbf{x} \end{aligned}$$

where the Heaviside step function $H$ is used in a similar manner as in [45] or [46]. Unlike in the explicit case, the regularity condition in eq. (12) has no impact on the implementation of band integrals in the implicit case. Due to the geometric nature of level sets, there is no need to compute any length element and the curvature does not intervene in the computation of band integrals. Indeed, considering the sign of $\psi$, pixels belonging to $\mathcal{B}_{\text{in}}$ or $\mathcal{B}_{\text{out}}$ are easily determined by dilating the front with the circular window $\mathcal{W}_B$. Regarding the average intensity along outward normal lines, we rely on the curvature-based formulation of the explicit curve:

$$\begin{aligned} & h_{\text{out}}(\mathbf{x}) = \\ & \frac{2}{B(2+B\kappa_\psi(\mathbf{x}))} \int_0^B I(\mathbf{x} + b\mathbf{n}_\psi(\mathbf{x}))(1+b\kappa_\psi(\mathbf{x}))db \end{aligned}$$

where the unit outward normal to the front at $\mathbf{x}$ is:

$$\mathbf{n}_\psi(\mathbf{x}) = \frac{\nabla\psi(\mathbf{x})}{\|\nabla\psi(\mathbf{x})\|}$$

This last expression is only adequate when $\mathbf{x}$ is located on the zero-level front. Computed as is, to maintain $\mathbf{n}_\psi$ normal to the front, $\psi$ should remain a distance function. This implies to update $\psi$ as a signed euclidean distance in the neighborhood of the front before estimating normal vectors. Regardless of the dimension of $\psi$, the curvature is expressed in terms of divergence:

$$\kappa_\psi(\mathbf{x}) = \text{div}\left( \frac{\nabla\psi(\mathbf{x})}{\|\nabla\psi(\mathbf{x})\|} \right)$$

which allows to write the level-set formulation of the second region term. From eq. (19), it follows:

$$\begin{aligned} & E_{\text{region}_2}[\psi] = \\ & \iint_{\mathcal{D}} H(\psi(\mathbf{x})+B)(1-H(\psi(\mathbf{x})))(I(\mathbf{x})-k_{\text{in}})^2 d\mathbf{x} + \\ & \iint_{\mathcal{D}} \delta(\psi(\mathbf{x})) \int_0^B \left(I(\mathbf{x}+b\mathbf{n}_\psi(\mathbf{x})) - h_{\text{out}}(\mathbf{x})\right)^2 (1+b\kappa_\psi(\mathbf{x})) db d\mathbf{x} \end{aligned}$$

For a point $\mathbf{x}$ located on the front, the speeds corresponding to the narrow band region terms are:

$$\begin{aligned} F_{\text{region}_1}(\mathbf{x}) &= (I(\mathbf{x})-k_{\text{out}})^2 - (I(\mathbf{x})-k_{\text{in}})^2 \\ F_{\text{region}_2}(\mathbf{x}) &= (I(\mathbf{x})-h_{\text{out}}(\mathbf{x}))^2 - (I(\mathbf{x})-k_{\text{in}})^2 \end{aligned}$$

On the implicit 2D contour, the curvature may be expanded as

$$\kappa_\psi = \frac{\psi_{xx}\psi_y^2 - 2\psi_x\psi_y\psi_{xy} + \psi_x^2\psi_{yy}}{(\psi_x^2+\psi_y^2)^{3/2}}$$

According to [47], the mean and gaussian curvatures of the implicit surface are:

$$\begin{aligned}\kappa_{\mathrm{M}\psi} &= \frac{\psi_{xx}(\psi_y^2+\psi_z^2)+\psi_{yy}(\psi_x^2+\psi_z^2)+\psi_{zz}(\psi_x^2+\psi_y^2)}{(\psi_x^2+\psi_y^2+\psi_z^2)^{3/2}} \\ &\quad -2\frac{\psi_{xy}\psi_x\psi_y+\psi_{xz}\psi_x\psi_z+\psi_{yz}\psi_y\psi_z}{(\psi_x^2+\psi_y^2+\psi_z^2)^{3/2}} \\ \kappa_{\mathrm{G}\psi} &= \frac{\sum_{(i,j,k)\in C}\psi_i^2(\psi_{jj}\psi_{kk}-\psi_{jk}^2)+2\psi}{(\psi_x^2+\psi_y^2+\psi_z^2)^2}\end{aligned}$$

where $C=\{(x,y,z),(y,z,x),(z,x,y)\}$ is the set of circular shifts of $(x,y,z)$. Eventually, the reader may note that the bias technique used in the explicit implementation is also applied in the level set model. The level set function $\psi$ evolves according to the narrow band technique [4], so that only pixels located in the neighborhood of the front are treated.

## 7. Results and discussion

Regarding the results, we should first point out that the goal of our experiments is not to compare explicit and implicit implementations, since it is well accepted that both exhibit their own advantages. These ones are typically topological and geometrical freedom for level sets. On the other hand, explicit approaches with polygonal snakes and triangular meshes yield less computational cost than level set and allow more control. The purpose of our tests is to compare the behavior of active contours and surfaces endowed with different data terms, on both explicit and implicit implementations. We intend to show the interest of the narrow band approach regardless of the implementation. To do so, the narrow band region energies are compared with an edge term, the global region term of the Chan-Vese model [11] as well as the combined term by Kimmel [23]. For every data term involved, we used the same smoothness term. Hence, the full energy is obtained by replacing $E_{\mathrm{region}}$ with the following data terms in eq. (3). The edge term is based on the image gradient magnitude:

$$E_{\mathrm{edge}}[\Gamma] = -\int_\Omega \|\nabla I(\mathbf{c})\|\,du + \alpha \iint_{R_{\mathrm{in}}} d\mathbf{x}$$

where $\alpha$ weights an additional balloon force [35] increasing the capture range. It allows the contour to be initialized far from the target boundaries, similarly to a region-based contour. The following global region energy is equivalent to the data term of the Chan-Vese model [11] described in eq. (1):

$$\begin{aligned}E_{\mathrm{global}}[\Gamma] &= \lambda \iint_{R_{\mathrm{in}}} (I(\mathbf{x})-k_{\mathrm{in}})^2 d\mathbf{x} \\ &\quad +(2-\lambda)\iint_{R_{\mathrm{out}}} (I(\mathbf{x})-k_{\mathrm{out}})^2 d\mathbf{x}\end{aligned}$$

Weights on inner and outer integrals are expressed in terms of a single parameter $\lambda$, since the full data term is already weighted by $(1-\omega)$. In subsequent experiments, the asymmetric configuration ($\lambda \neq 1$) will be explicitly indicated. Otherwise, the symmetric configuration is used. The data term of the combined model by Kimmel [23] holds a robust alignment term, encouraging intensity variations normal to the curve, and a symmetric global region term:

$$\begin{aligned}E_{\mathrm{combined}}[\Gamma] &= -\int_\Omega |\langle \nabla I(\mathbf{c}), \mathbf{n}\rangle|\,du \\ &\quad +\beta\left(\iint_{R_{\mathrm{in}}} (I(\mathbf{x})-k_{\mathrm{in}})^2 d\mathbf{x} + \iint_{R_{\mathrm{out}}} (I(\mathbf{x})-k_{\mathrm{out}})^2 d\mathbf{x}\right)\end{aligned}$$

For the edge and combined data terms, image gradient $\nabla I$ is computed on data convolved with first-order derivative of gaussian, where scale $s$ is empirically chosen to yield the most significant edges. The choice of $s$ is a tradeoff between noise removal and edge sharpness. The variational derivatives of the previous terms are:

$$\begin{aligned}\frac{\delta E_{\mathrm{edge}}}{\delta\Gamma} &= -\nabla\|\nabla I(\mathbf{c})\| - \alpha\mathbf{n} \\ \frac{\delta E_{\mathrm{global}}}{\delta\Gamma} &= [-\lambda(I(\mathbf{c})-k_{\mathrm{in}})^2 + (2-\lambda)(I(\mathbf{x})-k_{\mathrm{out}})^2]\mathbf{n} \\ \frac{\delta E_{\mathrm{combined}}}{\delta\Gamma} &= -\mathrm{sign}(\langle\nabla I(\mathbf{c}),\mathbf{n}\rangle)\nabla^2 I(\mathbf{c})\mathbf{n} \\ &\quad +\beta[-(I(\mathbf{c})-k_{\mathrm{in}})^2 + (I(\mathbf{c})-k_{\mathrm{out}})^2]\mathbf{n}\end{aligned}$$

We perform segmentation of visually uniform structures. Since we are looking for perceptually homogeneous objects, segmentation quality can be assessed visually. One can reasonably admit that the target object corresponds to the area containing the major part of the initial region. For all 2D datasets, the model, whether it is our explicit contour or the level set, is initialized as a small circle fully or partially inside the area of interest, far from the target boundaries. Similarly, for 3D images, our active surface and the 3D level set are initialized as small spheres. On a given image, a common initialization is used for all models. The initial curve is depicted for some experiments. In all subsequent figures, explicit contours and surfaces are drawn in red whereas implicit ones appear in blue.

For all experiments, the regularization weight $\omega$ is set to 0.5. The standard deviation of the gaussian smooth $\sigma$ takes its values between 1 and 2, which achieves the best regularization for all tested images. On noisy data, we

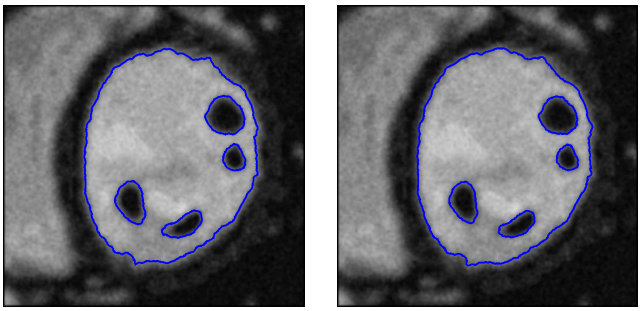

Global Narrow band 1

Figure 8: Left ventricle in MRI with level set

found that contours and surfaces with lower $\sigma$ are prone to boundary leaking. In addition, insufficient regularization makes level set implementations leave spurious isolated pixels inside and outside the inner region. Conversely, values above 2 might prevent the surface from propagating into narrow structures, like thin blood vessels. Moreover, since the width of the gaussian mask is proportional to $\sigma$, large standard deviations lead to significant increase of computational cost, especially for 3D segmentation.

Fig. 7 shows segmentation results of the brain ventricle in a 2D axial MRI (Magnetic Resonance Imaging) slice. As it is the case with many medical datasets, the partially blurred boundaries between ventricle and gray matter prevent the extraction of reliable edges in places. For the edge-based model, we could not find a suitable balloon weight $\alpha$ and gradient scale $s$ preventing the contour from being trapped in spurious noisy edges inside the shape while stopping on the actual boundaries. As regards combined and symmetric global approaches (see columns 2 and 4), the contour did not manage to grow, as inner and outer average intensities were not sufficiently different. Setting $\lambda$ to 0.9, we decrease the significance of inner deviation to the benefit of outer deviation, consequently allowing the contour to grow. As depicted in column 3, the contour undesirably flows into the gray matter part as soon as this area is reached, which is inconsistent with the initialization in our context. In this column, one may note that the drawn curves are not the final ones, but intermediate states to illustrate the leaking effect. Indeed, on this particular dataset, gray/white separation is the most probable partition with respect to a global two-class segmentation.

We also tested the snake on slices of the human heart in short-axis view, where the shape of the endocardium, i.e. the inner wall of the left ventricle, should be recovered. The slices were extracted from 3D+T MRI sequences. Finding the endocardium boundary is made more complex by the presence of papillary muscles, appearing as small dark areas inside the blood pool, as shown in fig. 8. This requires topological changes, hence

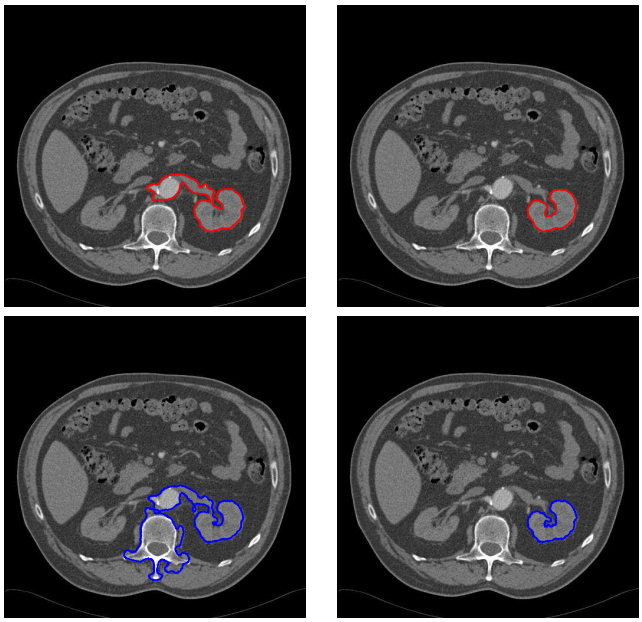

Global Narrow band 1

Figure 9: Kidney in abdominal CT with parametric contour (top) and level set (bottom)

only the implicit method was tested on this dataset. In order to keep a critical eye on our approach, we draw the attention on its equivalence with the Chan-Vese model on this particular image. The background is not uniform but still significantly darker than the target object. Thus, the classical region speed manages to make the front stabilize on the actual boundaries. Fig. 8 depicts the typical case in which there is no particular benefit in using the narrow band region energy.

In fig. 9 and 10, we illustrate the recovery of the kidney and aorta inner walls, respectively, in 2D CT (Computed Tomography) data. The global region energy makes the contour leak outside the target object, into neighboring structures of rather light gray intensity. Indeed, since the black background occupies a large area of the image, every bright grayscale is considered as a part of inner statistics. Conversely, the narrow band energy, which ignores the major part of the background, has a more local view and manages to keep the contour inside the kidney and the aorta. One may note that all segmented objects of interest are homogeneous. It has no incidence if we consider the inner band or the whole inner region for the homogeneity criterion in $E_{\text{region}_1}$. Indeed, in the region force of eq. (53), descriptor $k_{\text{in}}$ may be equally the average intensity on $R_{\text{in}}$ or $\mathcal{B}_{\text{in}}$.

The band thickness $B$ is an important parameter of our method and should be discussed. Apart from its impact on the algorithmic complexity - computing average intensities $\mu(\mathcal{B}_{\text{in}})$ and $\mu(\mathcal{B}_{\text{out}})$ takes at least $O(nB)$ oper-

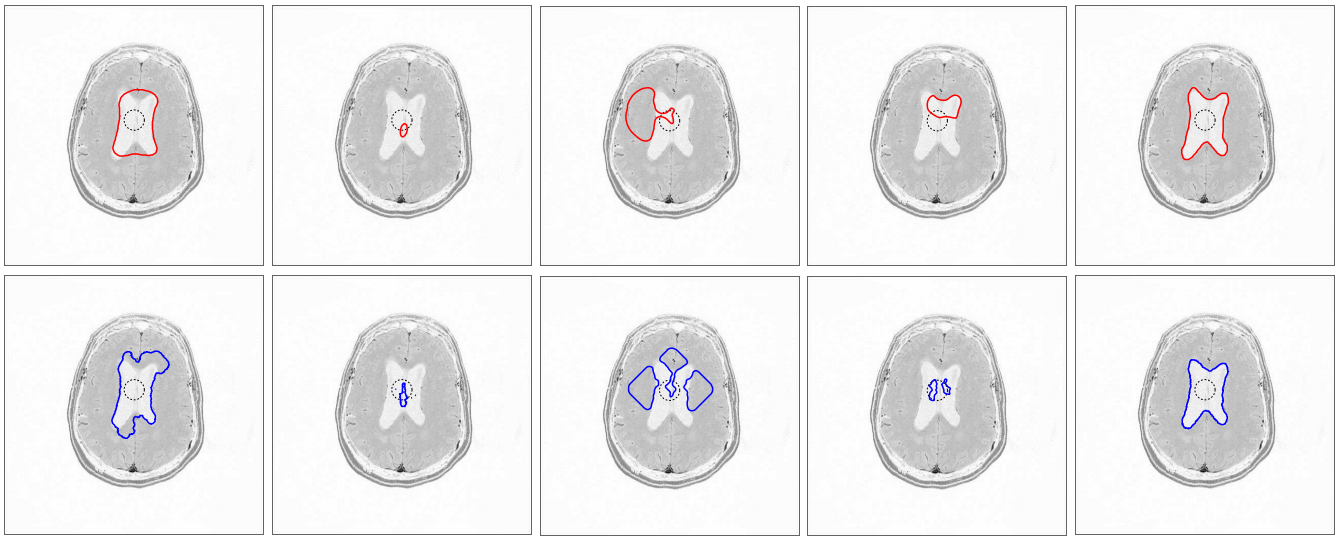


Figure 7: Brain ventricle in 2D axial MRI, with parametric contour (top) and level set (bottom). The initial curve is drawn in black dashed line

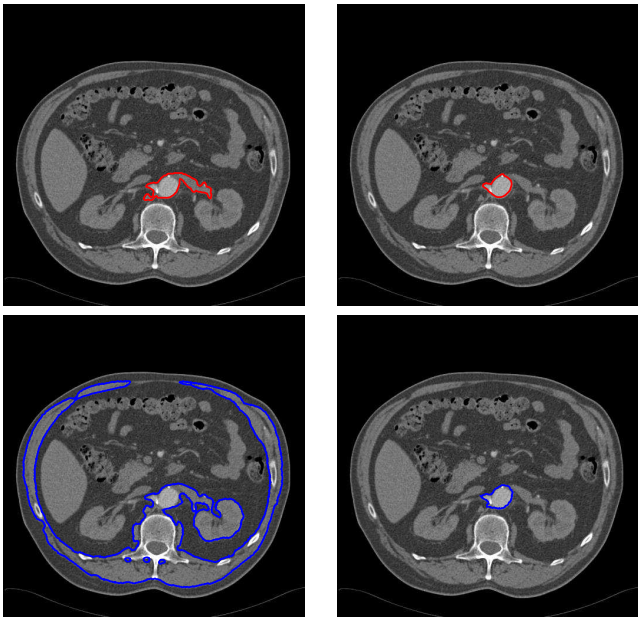


Figure 10: Aorta in abdominal CT with parametric contour (top) and level set (bottom)

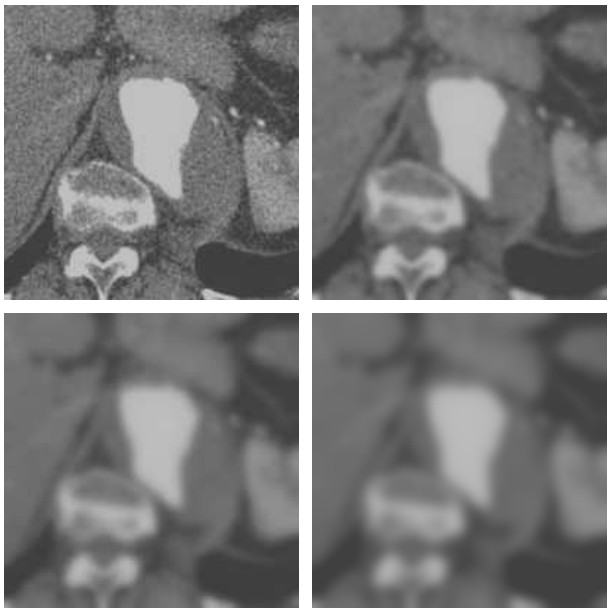

Figure 11: Succesive gaussian smoothings of an axial slice of 3D CT data

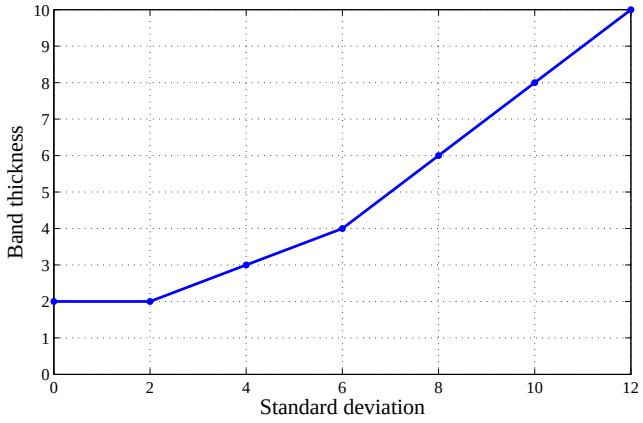


Figure 12: Minimal band thickness versus standard deviation of gaussian smoothing

ations - it controls the trade-off between local and global features around the object. If $B = 1$, the region energy is as local as an edge term whereas if $B$ goes to infinity, it is equivalent to the global region term. The main image property having an effect on the minimal band thickness is the edges sharpness. Indeed, the deformable needs a larger band as the boundaries of the target object are fuzzy. To put this phenomenon into evidence, we apply the active contour on an increasingly blurred image, as depicted in fig. 11. Fig. 12 represents the requested minimal band thickness versus the standard deviation of gaussian smoothing. Bands thinner than the minimal one yield boundary leakage into neighboring structures. The original image can be segmented with a 2 pixel-wide band. For subsequent images, increasing the band turns out to be necessary. One may assume that the blur level of the last image in the sequence is rarely encountered in the applications we aim at, we choose $B = 10$ in our experiments.

We now describe results obtained on color images, shown in fig. 13. The initial position, which is equal for every tested model, is indicated by a dashed circle. In the previous experiments, the outer neighborhoods of target objects were nearly uniform, enabling the use of the first narrow band region energy. This condition is not met in these datasets and we thus prove the interest of our second narrow band region energy. The minimal variance principle is easily extended to vector-valued images, by rewriting the region energies with vector quantities. Let us consider the vector-valued image $\mathbf{I}$ - holding, for instance, the RGB components - and vector descriptors $\mathbf{k}_{\text{in}}$ and $\mathbf{k}_{\text{out}}$. In the inner term, the integrand becomes $\|\mathbf{I}-\mathbf{k}_{\text{in}}\|^2$ and similarly for the outer term. The artificial image in the top row of fig. 13, made up of color ellipses corrupted with gaussian noise, is segmented using RGB values. Due to the averaging performed on the outer region and band respectively, the global region term and the first narrow band term split the image with respect to the blue component, since it is the dominant color in the background and it does not occur in the inner region.

The images depicted in the second and third row holds perceptually color-uniform objects. They were segmented using the UV chrominance components of the YUV color space. Neglecting the luminance Y makes color statistics insensitive to illumination changes in visually uniform regions, allowing to handle highlights and shadows properly. For other recent work on active contours and level sets in color images, the reader may refer to [48, 49, 50]. As previous, the second narrow band energy does not perform any averaging on the outer band. It preserves spatial independence in the outer neighborhood along the curve, unlike other region terms. One should note that objects well segmented with the first narrow band region energy can also be segmented with the second one, whereas the opposite is false. On these datasets, the combined model also performs good segmentation, as reliable edges can be extracted. The gradient alignment energy acts as a stopping term and hence compensates the growth induced by the region term. Computational times imputed to the explicit contour fall between 0.5s and 1s for 2D images, which average size is 512 $\times$ 512, with a C++ implementation running on an Intel Core 2 Duo 2GHz with 1Gb RAM. On the same images, level-set implementations are twice to third times slower.

Models endowed with global region terms are inherently affected by modification of the background, even if changes arise in areas not related to the boundary of the object. In figures numbered from 14 to 17, we put this phenomenon into evidence by showing the evolution of the contour with the different data terms, on an initial image and a tagged image. 20 iterations of gradient descent are performed between each frame. In fig. 14, the global region approach flows into the neighboring blue block, since it is considered as the most different area from the whole background. Tagging the image, and hence modifying background features in a significant manner, yields a much different behavior. In fig. 15, the homogeneity criterion is made asymmetric by increasing $\lambda$ to 1.1. In this way, the model is less permissive with respect to inner deviation, which limits the growth effect. On the initial image, it turned out to be impossible to find a suitable $\lambda$ making the curve stop on the desired boundaries, as inner and outer statistics were not sufficiently different. The same phenomenon arises with the combined model in fig. 16, as no tradeoff $\beta$ between edge and region term could be found to properly recover the desired object. The purpose of this particular experiment is twofold. On the one hand, we demonstrate that specific image configurations prevent the use of global region terms. On the other hand, the ability to recover a target object is influenced by modifications external to this object, which may be an undesirable feature for real applications.

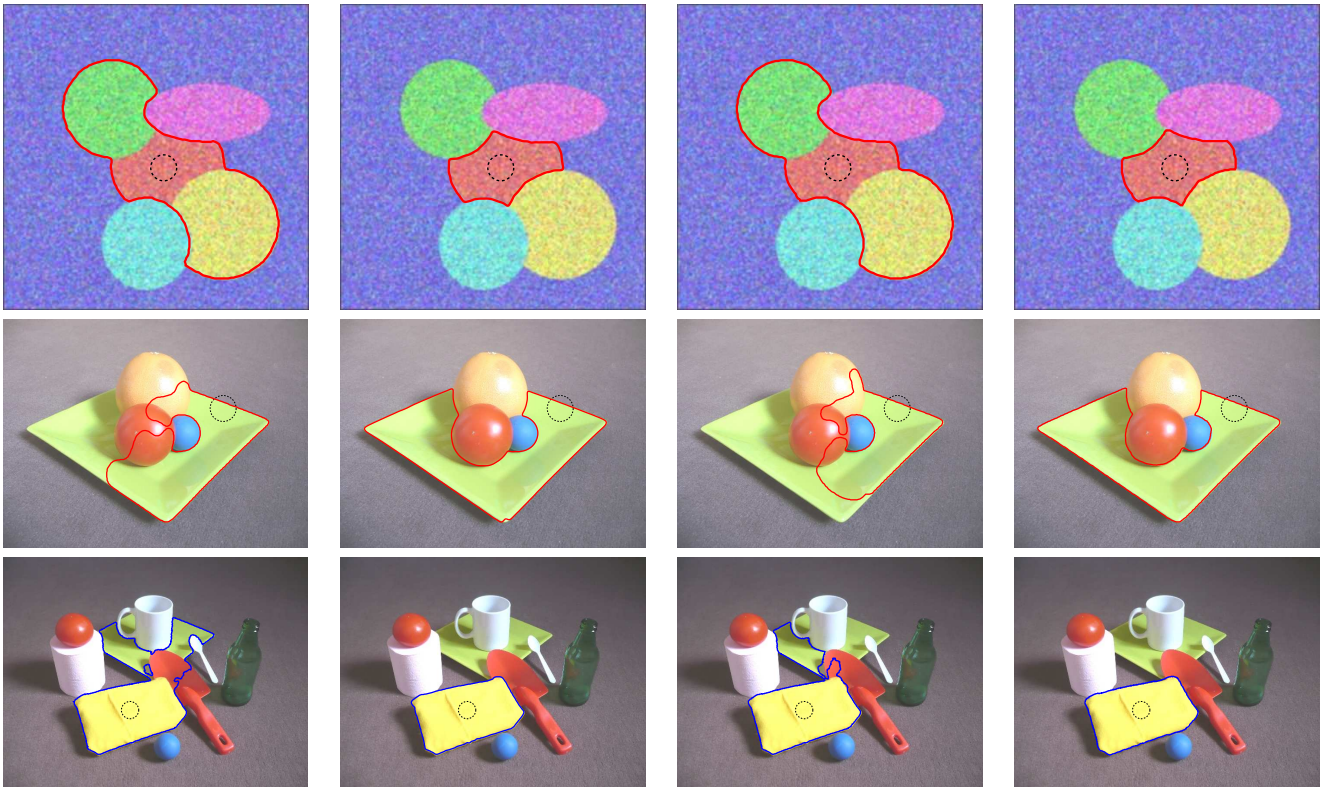


Figure 13: Segmentation of color artificial image (first row) and photographs (second and third rows). The initial curve is drawn in black dashed line

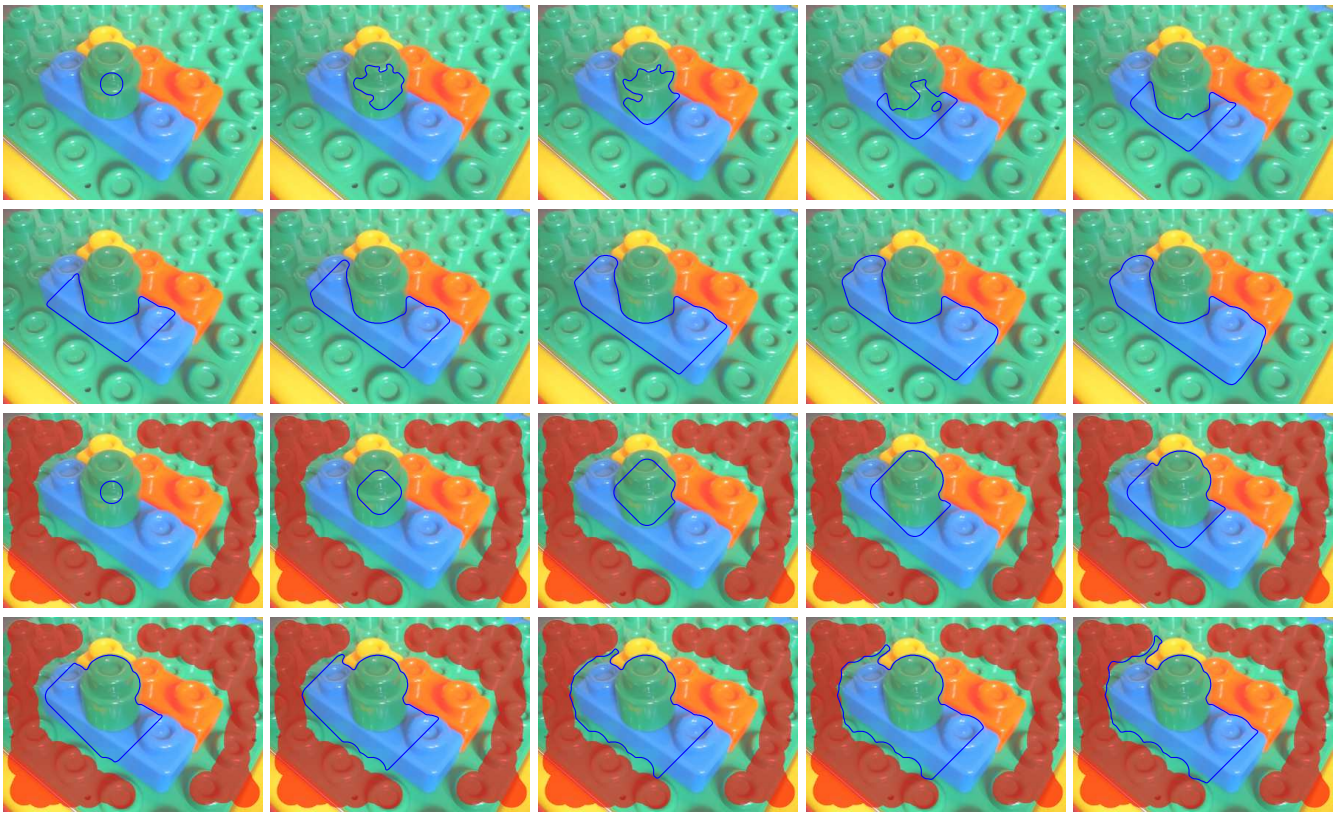

Figure 14: Evolution with symmetric global region term

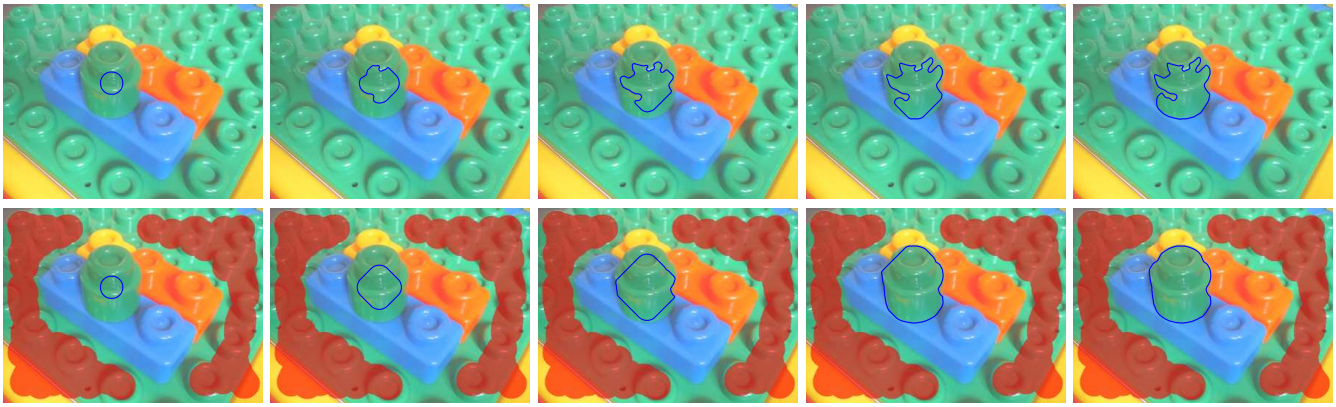

Figure 15: Evolution with asymmetric global region term ($\lambda = 1.1$)

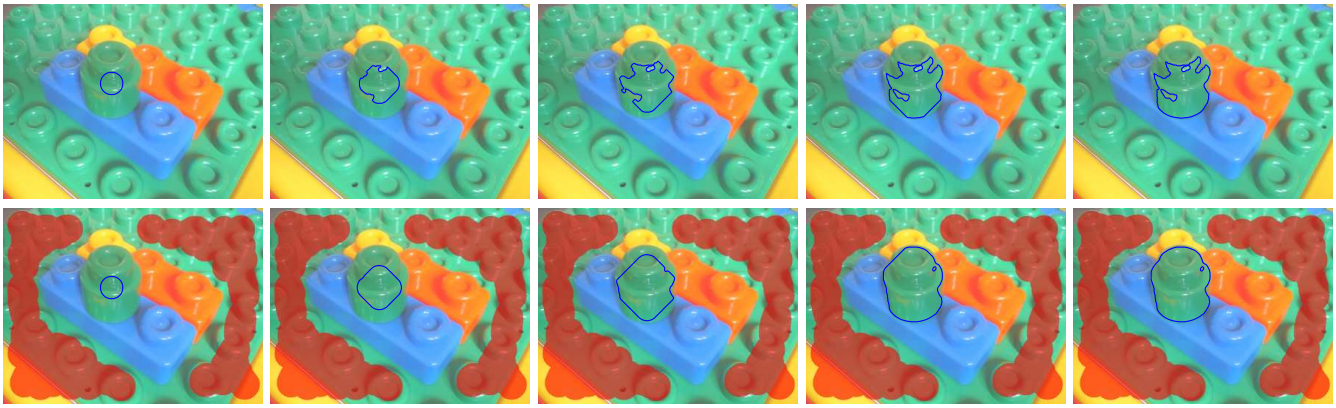

Figure 16: Evolution with combined term

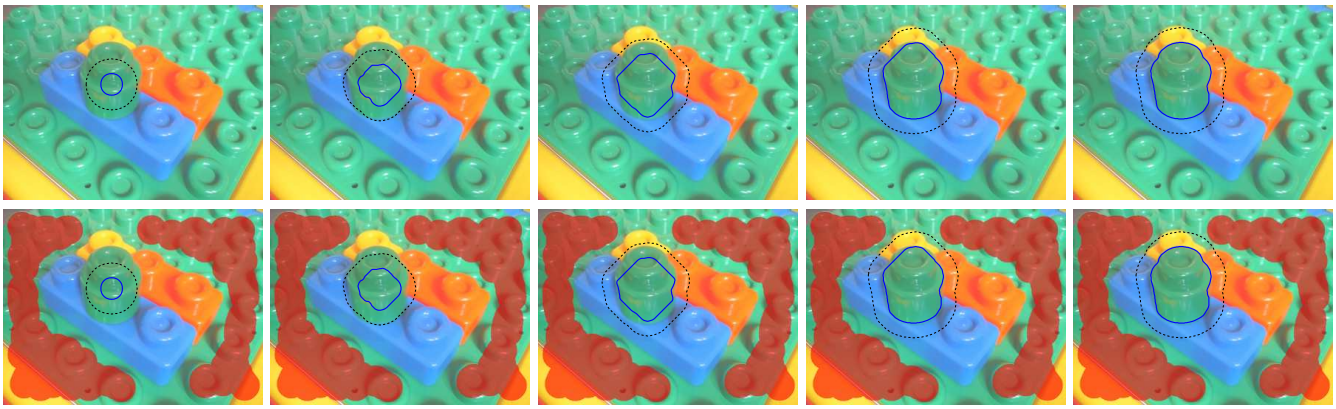

Figure 17: Evolution with first narrow band region term. The outer parallel curve $\Gamma_{[-B]}$ is drawn in black dashed line

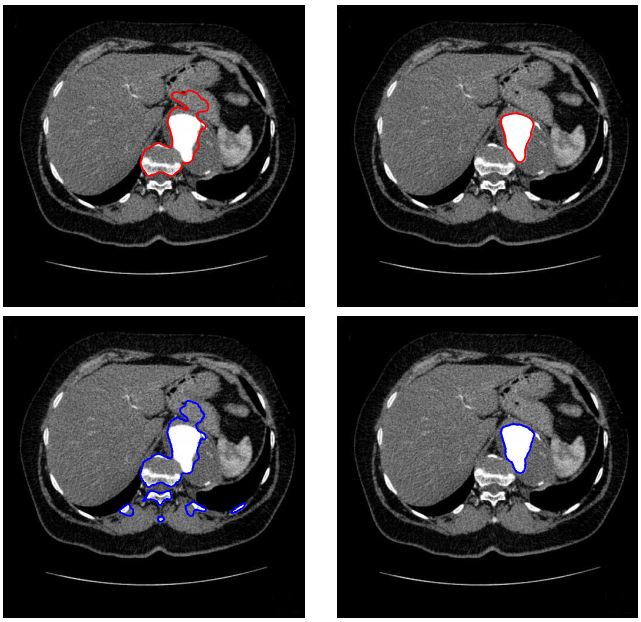

Global Narrow band 1

Figure 18: Slices of deformable mesh (top) and 3D level set surface (bottom) on axial planes of a 3D abdominal CT

We eventually describe experiments made with the active surface model on 3D CT datasets of the abdomen. The surface is used to segment the inside of the whole aorta, in the context of abdominal aortic aneurysm diagnosis. It is initialized as a sphere totally inside the vessel and inflated afterwards. These experiments emphasize the ability of our explicit active surface to explore tree-like structures with narrow paths while keeping sufficient regularity. Endowed with the global region-term, we observe the same phenomenon as with the active contour in 2D CT images. The surface tends to flow into neighboring structures which have a significantly brighter intensity than the background, especially when areas are separated by thin boundaries. On this data, such case appears between the white blood aorta and vertebrae. Fig. 18 shows an axial slice of a 3D abdominal CT dataset whereas the 3D representation appears in fig. 19. The image size is $512 \times 512 \times 800$, yielding a computational time of nearly 55s for the deformable mesh and more than 3mn for the implicit surface.

## 8. Conclusion

We have presented in this paper a narrow band region approach for deformable contours and surfaces driven by energy minimization. The approach is based on two novel region terms, formulating a homogeneity criterion in inner and outer bands neighboring the evolving curve or surface. The first and second term relies on the asumption of a respectively uniform and piecewise uniform background in

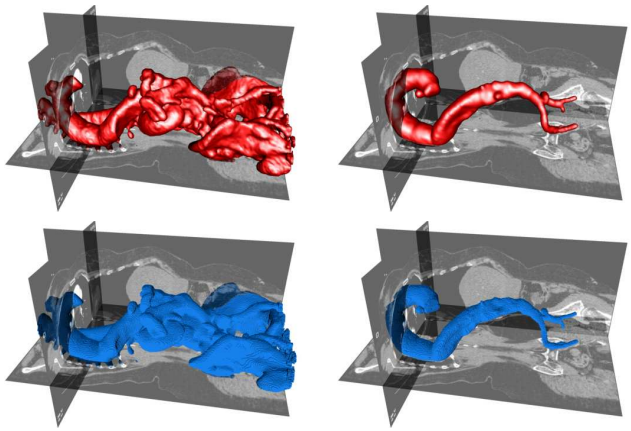

Global Narrow band 1

Figure 19: Deformable mesh (top) and 3D level set surface (bottom) in 3D abdominal CT

the vicinity of the target object. Based on the theory of parallel curves and surfaces, a mathematical development was carried out in order to express the region energies in a form allowing natural implementation on explicit models. The distinctive feature of the 2D region term resides in curvature. By extension, the region term employed in the 3D mesh uses mean and gaussian curvatures. The narrow band region energy managed to overcome the drawbacks of deformable models relying exclusively on edge terms or global region terms. We provided explicit and level-set based implementations in 2D and 3D. Very promising results were obtained on grayscale and color images.

Several improvements will be considered in the near future. First, the bias added to the region force, described in section 5.5, comes more from empirical observations rather than rigorous calculus of energy variations. Narrow band region-based models have a diminished capture range and the bias prevents the model to be stuck in a local minimum when inner and outer statistics are similar. Future work may concentrate on exploiting both global and band-based region features, in order to dispense the use of such bias. Moreover, further investigations will be performed in embedding narrow region terms into more geometrically constrained models, like the deformable generalized cylinder in [51]. We also plan to extend the model to temporal segmentation, in order to track evolving objects in videos, and to textured images [25]. Finally, automated learning of the energy weights and band thickness, with respect to a given class of images, could be considered.

## A. Transformation of area and volume integrals

In this appendix, we provide details about the transformations of area and volume integrals over 2D and 3D bands, respectively. These transformations lead to mathematical expressions which discretized forms are convenient to implement on explicit active contours and surfaces.

*A.1. Area integral over 2D band*

We give a general form for an area integral over a band $\mathcal{B}$ bounded by two non-intersecting simple curves $\Gamma_1$ and $\Gamma_2$, as depicted in fig. 4. The curves enclose regions $R_1$ and $R_2$, respectively. According to Green's theorem, since $\mathcal{B} = R_1 \backslash R_2$, the integral of a $\mathbb{R}^2 \to \mathbb{R}$ function $f$ over $\mathcal{B}$ is:

$$\begin{aligned} J(f,\mathcal{B}) &= J(f,R_1) - J(f,R_2) \\ &= \int_\Omega x_{1u} P(\mathbf{c}_1) + y_{1u} Q(\mathbf{c}_1) du \\ &- \int_\Omega x_{2u} P(\mathbf{c}_2) + y_{2u} Q(\mathbf{c}_2) du \end{aligned}$$

where $P$ and $Q$ are the anti-derivatives defined in eq. (13). We gather the terms depending on $P$ and $Q$:

$$\begin{aligned} J(f,\mathcal{B}) &= \int_\Omega x_{1u} P(\mathbf{c}_1) - x_{2u} P(\mathbf{c}_2) du \\ &+ \int_\Omega y_{1u} Q(\mathbf{c}_1) - y_{2u} Q(\mathbf{c}_2) du \end{aligned}$$

We introduce a family of curves $\{\tilde{\Gamma}(\alpha)\}_{\alpha\in[0,1]}$ interpolating from $\Gamma_1$ to $\Gamma_2$. The position vector of a given curve $\tilde{\Gamma}(\alpha)$ is

$$\tilde{\mathbf{c}}(\alpha,u) = (1-\alpha)\mathbf{c}_2(u) + \alpha \mathbf{c}_1(u)$$

This property allows us to write:

$$\begin{aligned} x_{1u} P(\mathbf{c}_1) - x_{2u} P(\mathbf{c}_2) &= \Big[\tilde{x}_u P(\tilde{\mathbf{c}})\Big]_{\alpha=0}^{\alpha=1} \\ &= \int_0^1 \frac{d}{d\alpha}\Big\{\tilde{x}_u P(\tilde{\mathbf{c}})\Big\}\, d\alpha \end{aligned}$$

and similarly for $y_{1u}Q(\mathbf{c}_1) - y_{2u}Q(\mathbf{c}_2)$. We have:

$$\begin{aligned} J(f,\mathcal{B}) &= \int_\Omega \int_0^1 \frac{d}{d\alpha}\Big\{\tilde{x}_u P(\tilde{\mathbf{c}}) + \tilde{y}_u Q(\tilde{\mathbf{c}})\Big\}\, d\alpha du \\ &= \int_\Omega \int_0^1 \tilde{x}_{\alpha u} P(\tilde{\mathbf{c}}) + \tilde{y}_{\alpha u}) Q(\tilde{\mathbf{c}}) d\alpha du \\ &+ \int_\Omega \int_0^1 \tilde{x}_u \left\langle \tilde{\mathbf{c}}_\alpha, \nabla P(\tilde{\mathbf{c}})\right\rangle + \tilde{y}_u \left\langle \tilde{\mathbf{c}}_\alpha, \nabla Q(\tilde{\mathbf{c}})\right\rangle d\alpha du \end{aligned}$$

with $\tilde{\mathbf{c}}_\alpha = \mathbf{c}_1 - \mathbf{c}_2$. Integrating by parts the term depending on $P$ with respect to $u$, we obtain:

$$\begin{aligned} \int_\Omega \tilde{x}_{\alpha u} P(\tilde{\mathbf{c}}) du &= \Big[\tilde{x}_\alpha P(\tilde{\mathbf{c}})\Big]_{u=0}^{u=1} \\ &- \int_\Omega \tilde{x}_\alpha \frac{d}{du}\Big\{P(\tilde{\mathbf{c}})\Big\}\, du \end{aligned}$$

Since $\Gamma_1$ and $\Gamma_2$ are closed curves, resulting in $\mathbf{c}_1(0) = \mathbf{c}_1(1)$ and $\mathbf{c}_{1u}(0) = \mathbf{c}_{1u}(1)$ and similarly for $\mathbf{c}_2$, the boundary term vanish:

$$\int_\Omega \tilde{x}_{\alpha u} P(\tilde{\mathbf{c}}) du = -\int_\Omega \tilde{x}_\alpha \left\langle \tilde{\mathbf{c}}_u, \nabla P(\tilde{\mathbf{c}})\right\rangle du$$

We apply the same derivation on the term depending on $Q$, which results in:

$$\begin{aligned} J(f,\mathcal{B}) &= \int_\Omega \int_0^1 \left\langle \nabla P(\tilde{\mathbf{c}}), \tilde{x}_u \tilde{\mathbf{c}}_\alpha - \tilde{x}_\alpha \tilde{\mathbf{c}}_u\right\rangle d\alpha du \\ &+ \int_\Omega \int_0^1 \left\langle \nabla Q(\tilde{\mathbf{c}}), \tilde{y}_u \tilde{\mathbf{c}}_\alpha - \tilde{y}_\alpha \tilde{\mathbf{c}}_u\right\rangle d\alpha du \end{aligned}$$

Using simplifications

$$\frac{\partial P}{\partial y} = -\frac{1}{2} f \qquad \frac{\partial Q}{\partial x} = \frac{1}{2} f,$$

and rewriting with cross product, the final expression of the area integral is

$$J(f,\mathcal{B}) = \int_\Omega \int_0^1 f(\tilde{\mathbf{c}})(\mathbf{c}_1 - \mathbf{c}_2) \times \tilde{\mathbf{c}}_u d\alpha du \qquad (58)$$

*A.2. Area integral over inner band*

We apply the general result in eq. (58) on inner band $\mathcal{B}_{\text{in}}$, considering curves $\Gamma$ and $\Gamma_{[B]}$ instead of $\Gamma_1$ and $\Gamma_2$. Equations 7 and 11 give the substitutions:

$$\begin{aligned} \mathbf{c}_1 &= \mathbf{c} \\ \mathbf{c}_2 &= \mathbf{c} + B\mathbf{n} \\ \mathbf{c}_{1u} &= \mathbf{c}_u \\ \mathbf{c}_{2u} &= (1 - B\kappa)\mathbf{c}_u \end{aligned}$$

Using the identity $\mathbf{c}_u \times \mathbf{n} = -\mathbf{n} \times \mathbf{c}_u = \ell$, we obtain:

$$\begin{aligned} &(\mathbf{c}_1 - \mathbf{c}_2) \times ((1-\alpha)\mathbf{c}_{2u} + \alpha \mathbf{c}_{1u}) \\ &= (\mathbf{c} - (\mathbf{c} + B\mathbf{n})) \times ((1-\alpha)(1-B\kappa)\mathbf{c}_u + \alpha \mathbf{c}) \\ &= B\ell(B\kappa(\alpha - 1) - 1) \end{aligned}$$

Combined with eq. (16), this result yields:

$$J(f,\mathcal{B}_{\text{in}}) = \int_\Omega \int_0^1 f(\mathbf{c} + B(\alpha-1)\mathbf{n}) B\ell(B\kappa(\alpha-1)-1) d\alpha du$$

Introducing a variable thickness $b = B(1-\alpha)$, ( $d\alpha = -db \,/\, B$ ), we finally get:

$$J(f,\mathcal{B}_{\text{in}}) = \int_\Omega \int_0^B f(\mathbf{c} + b\mathbf{n})\ell(1 - b\kappa) db du$$

*A.3. Volume integral over 3D band*

We give a general form for an area integral over a volumic band $\mathcal{B}$ bounded by two non-intersecting surfaces $\Gamma_1$ and $\Gamma_2$, enclosing regions $R_1$ and $R_2$, respectively. The mathematical derivation presented here may be considered as the 3D extension of appendix A.1. Region $R_2$ is fully contained into $R_1$, such that $\mathcal{B} = R_1 \backslash R_2$. According to the divergence theorem described in eqs. (30) and (32), the integral of a $\mathbb{R}^3 \to \mathbb{R}$ function $f$ over $\mathcal{B}$ is:

$$\begin{aligned} J(f,\mathcal{B}) &= J(f,R_1) - J(f,R_2) \\ &= \iint_{\Omega^2} \left\langle \mathbf{F}(\mathbf{s}_2(u,v)), \mathbf{s}_{2u} \times \mathbf{s}_{2v}\right\rangle du dv \\ &- \iint_{\Omega^2} \left\langle \mathbf{F}(\mathbf{s}_1(u,v)), \mathbf{s}_{1u} \times \mathbf{s}_{1v}\right\rangle du dv \end{aligned}$$

where $\mathbf{F}$ is the vector field $[P\ Q\ R]^T$ defined in eq. (33). Introducing a variable surface of position vector $\tilde{\mathbf{s}}(\alpha)$ interpolating from $\Gamma_1$ to $\Gamma_2$ as $\alpha$ varies from 0 to 1, such that

$$\tilde{\mathbf{s}}(\alpha,u,v) = (1-\alpha)\mathbf{s}_1(u,v) + \alpha\mathbf{s}_2(u,v),$$

we have:

$$\begin{aligned}&\langle \mathbf{F}(\mathbf{s}_2), \mathbf{s}_{2u}\times\mathbf{s}_{2v}\rangle - \langle \mathbf{F}(\mathbf{s}_1), \mathbf{s}_{1u}\times\mathbf{s}_{1v}\rangle \\ &= \Big[\mathbf{F}(\tilde{\mathbf{s}})\tilde{\mathbf{s}}_u\times\tilde{\mathbf{s}}_v\Big]_{\alpha=0}^{\alpha=1} = \int_0^1 \frac{d}{d\alpha}\Big\{\mathbf{F}(\tilde{\mathbf{s}})\tilde{\mathbf{s}}_u\times\tilde{\mathbf{s}}_v\Big\}\,d\alpha\end{aligned}$$

This yields:

$$J(f,\mathcal{B}) = \iiint_{\Omega^2}\int_0^1 \frac{d}{d\alpha}\Big\{\langle \mathbf{F}(\tilde{\mathbf{s}}), \tilde{\mathbf{s}}_u\times\tilde{\mathbf{s}}_v\rangle\Big\}\,d\alpha du dv$$

Using the product rule to expand the $\alpha$-derivative, $J(f,\mathcal{B})$ is split into two terms:

$$J(f,\mathcal{B}) = J_1 + J_2$$

Integral $J_1$ depends on the partial derivatives of $\mathbf{F}$:

$$J_1 = \iiint_{\Omega^2}\int_0^1 \left\langle \frac{d\mathbf{F}(\tilde{\mathbf{s}})}{d\alpha}, \tilde{\mathbf{s}}_u\times\tilde{\mathbf{s}}_v\right\rangle d\alpha du dv$$

where $d\mathbf{F}(\tilde{\mathbf{s}})/d\alpha$ is a vector, expressed using partial derivatives of application $\mathbf{F}$:

$$\begin{aligned}\frac{d\mathbf{F}(\tilde{\mathbf{s}})}{d\alpha} &= \left[\left\langle \frac{d\tilde{\mathbf{s}}}{d\alpha}, \nabla P\right\rangle\ \left\langle \frac{d\tilde{\mathbf{s}}}{d\alpha}, \nabla Q\right\rangle\ \left\langle \frac{d\tilde{\mathbf{s}}}{d\alpha}, \nabla R\right\rangle\right]^T \\ &= \nabla\mathbf{F}\tilde{\mathbf{s}}_\alpha\end{aligned}$$

where $\nabla\mathbf{F}$ is the following Jacobian matrix:

$$\nabla\mathbf{F} = \begin{bmatrix} \frac{\partial P}{\partial x} & \frac{\partial P}{\partial y} & \frac{\partial P}{\partial z} \\ \frac{\partial Q}{\partial x} & \frac{\partial Q}{\partial y} & \frac{\partial Q}{\partial z} \\ \frac{\partial R}{\partial x} & \frac{\partial R}{\partial y} & \frac{\partial R}{\partial z} \end{bmatrix} = \begin{bmatrix} \frac{1}{3}f & \frac{\partial P}{\partial y} & \frac{\partial P}{\partial z} \\ \frac{\partial Q}{\partial x} & \frac{1}{3}f & \frac{\partial Q}{\partial z} \\ \frac{\partial R}{\partial x} & \frac{\partial R}{\partial y} & \frac{1}{3}f \end{bmatrix}$$

Using matrix notation, we use the general rule

$$\mathbf{a}^T\mathbf{A}\mathbf{b} = (\mathbf{a}^T\mathbf{A}\mathbf{b})^T = \mathbf{b}^T\mathbf{A}\mathbf{a}$$

to rewrite the integrand of $J_1$ with inner product notation:

$$\langle \nabla\mathbf{F}\tilde{\mathbf{s}}_\alpha, \tilde{\mathbf{s}}_u\times\tilde{\mathbf{s}}_v\rangle = \langle \tilde{\mathbf{s}}_\alpha, \nabla\mathbf{F}^T\tilde{\mathbf{s}}_u\times\tilde{\mathbf{s}}_v\rangle$$

On the other hand, integral $J_2$ depends explicitly on $\mathbf{F}$:

$$\begin{aligned}J_2 &= \iiint_{\Omega^2}\int_0^1 \left\langle \mathbf{F}, \frac{d}{d\alpha}\Big\{\tilde{\mathbf{s}}_u\times\tilde{\mathbf{s}}_v\Big\}\right\rangle d\alpha du dv \\ &= \iiint_{\Omega^2}\int_0^1 \langle \mathbf{F}, \tilde{\mathbf{s}}_{\alpha u}\times\tilde{\mathbf{s}}_v\rangle + \langle \mathbf{F}, \tilde{\mathbf{s}}_u\times\tilde{\mathbf{s}}_{\alpha v}\rangle\, d\alpha du dv\end{aligned}$$

Since the scalar triple product is anti-symetrical, we have

$$J_2 = \iiint_{\Omega^2}\int_0^1 \langle \tilde{\mathbf{s}}_{\alpha u}, \tilde{\mathbf{s}}_v\times\mathbf{F}\rangle + \langle \tilde{\mathbf{s}}_{\alpha v}, \mathbf{F}\times\tilde{\mathbf{s}}_u\rangle\, d\alpha du dv$$

We integrate by parts the first and second terms with respect to $u$ and $v$, respectively:

$$\begin{aligned}J_2 &= \int_0^1\int_0^1 \Big[\langle \tilde{\mathbf{s}}_\alpha, \tilde{\mathbf{s}}_v\times\mathbf{F}\rangle\Big]_{u=0}^{u=1} d\alpha dv \\ &\quad - \iiint_{\Omega^2}\int_0^1 \left\langle \tilde{\mathbf{s}}_\alpha, \frac{d}{du}\Big\{\tilde{\mathbf{s}}_v\times\mathbf{F}\Big\}\right\rangle d\alpha du dv \\ &\quad + \int_0^1\int_0^1 \Big[\langle \tilde{\mathbf{s}}_\alpha, \mathbf{F}\times\tilde{\mathbf{s}}_u\rangle\Big]_{v=0}^{v=1} d\alpha du \\ &\quad - \iiint_{\Omega^2}\int_0^1 \left\langle \tilde{\mathbf{s}}_\alpha, \frac{d}{dv}\Big\{\mathbf{F}\times\tilde{\mathbf{s}}_u\Big\}\right\rangle d\alpha du dv\end{aligned}$$

The boundary terms vanish thanks to the surface parameterization, according to eq. (20) or (21). Expanding the cross product derivatives, we get:

$$\begin{aligned}J_2 &= -\iiint_{\Omega^2}\int_0^1 \left\langle \tilde{\mathbf{s}}_\alpha, \tilde{\mathbf{s}}_{uv}\times\mathbf{F} + \tilde{\mathbf{s}}_v\times\frac{d\mathbf{F}(\tilde{\mathbf{s}})}{du}\right\rangle d\alpha du dv \\ &\quad -\iiint_{\Omega^2}\int_0^1 \left\langle \tilde{\mathbf{s}}_\alpha, \frac{d\mathbf{F}(\tilde{\mathbf{s}})}{dv}\times\tilde{\mathbf{s}}_u + \mathbf{F}\times\tilde{\mathbf{s}}_{uv}\right\rangle d\alpha du dv \\ &= -\iiint_{\Omega^2}\int_0^1 \langle \tilde{\mathbf{s}}_\alpha, \tilde{\mathbf{s}}_v\times(\nabla\mathbf{F}\tilde{\mathbf{s}}_u) + (\nabla\mathbf{F}\tilde{\mathbf{s}}_v)\times\tilde{\mathbf{s}}_u\rangle\, d\alpha du dv\end{aligned}$$

In the previous equation, the second member of the inner product is expanded as a function of $\tilde{\mathbf{s}}_u\times\tilde{\mathbf{s}}_v$:

$$\begin{aligned}&\tilde{\mathbf{s}}_v\times(\nabla\mathbf{F}\tilde{\mathbf{s}}_u) + (\nabla\mathbf{F}\tilde{\mathbf{s}}_v)\times\tilde{\mathbf{s}}_u \\ &= \begin{bmatrix} -\frac{\partial Q}{\partial y} - \frac{\partial R}{\partial z} & \frac{\partial Q}{\partial x} & \frac{\partial R}{\partial x} \\ \frac{\partial P}{\partial y} & -\frac{\partial P}{\partial x} - \frac{\partial R}{\partial z} & \frac{\partial R}{\partial y} \\ \frac{\partial P}{\partial z} & \frac{\partial Q}{\partial z} & -\frac{\partial P}{\partial x} - \frac{\partial Q}{\partial y} \end{bmatrix} \tilde{\mathbf{s}}_u\times\tilde{\mathbf{s}}_v\end{aligned}$$

which is rewritten in a form containing the divergence of vector field:

$$\tilde{\mathbf{s}}_v\times(\nabla\mathbf{F}\tilde{\mathbf{s}}_u) + (\nabla\mathbf{F}\tilde{\mathbf{s}}_v)\times\tilde{\mathbf{s}}_u = \left(\nabla\mathbf{F}^T - \mathrm{div}(\mathbf{F})\mathbf{I}\right)\tilde{\mathbf{s}}_u\times\tilde{\mathbf{s}}_v$$

where $\mathbf{I}$ is the $3\times 3$ identity matrix. It yields, for integral $J_2$:

$$J_2 = \iiint_{\Omega^2}\int_0^1 \left\langle \tilde{\mathbf{s}}_\alpha, \left(\mathrm{div}(\mathbf{F})\mathbf{I} - \nabla\mathbf{F}^T\right)\tilde{\mathbf{s}}_u\times\tilde{\mathbf{s}}_v\right\rangle d\alpha du dv$$

As a result, $J_1$ and $J_2$ are now straightforward to add:

$$\begin{aligned} J(f,\mathcal{B}) &= J_1 + J_2 \\ &= \iiint_{\Omega^2}\int_0^1 \left\langle \tilde{\mathbf{s}}_\alpha \ , \ \nabla\mathbf{F}^T\tilde{\mathbf{s}}_u\times\tilde{\mathbf{s}}_v \right. \\ &\qquad \left. + \left(\mathrm{div}(\mathbf{F})\mathbf{I} - \nabla\mathbf{F}^T\right)\tilde{\mathbf{s}}_u\times\tilde{\mathbf{s}}_v \right\rangle d\alpha du dv \\ &= \iiint_{\Omega^2}\int_0^1 \mathrm{div}(\mathbf{F})\left\langle \tilde{\mathbf{s}}_\alpha, \tilde{\mathbf{s}}_u\times\tilde{\mathbf{s}}_v\right\rangle \ d\alpha du dv \end{aligned}$$

Eventually we give the final expression of the volume integral:

$$J(f,\mathcal{B}) = \iiint_{\Omega^2}\int_0^1 f(\tilde{\mathbf{s}})\left\langle \mathbf{s}_2-\mathbf{s}_1, \tilde{\mathbf{s}}_u\times\tilde{\mathbf{s}}_v\right\rangle \ d\alpha du dv \qquad (59)$$

This expression is intuitively understood as the scalar triple product is the volume of the infinitesimal parallelepiped spanned by vectors $\mathbf{s}_2-\mathbf{s}_1$, $\tilde{\mathbf{s}}_u$ and $\tilde{\mathbf{s}}_v$.

*A.4. Volume integral over 3D inner band*

We apply the result in eq. (59) on surfaces $\Gamma$ and $\Gamma_{[B]}$ instead of $\Gamma_1$ and $\Gamma_2$, in order to provide a general expression for $J(f,\mathcal{B}_{\mathrm{in}})$. Thanks to equations 24 and 28, we apply the substitutions:

$$\begin{aligned} \mathbf{s}_1 &= \mathbf{s} \\ \mathbf{s}_2 &= \mathbf{s} + B\mathbf{n} \\ \mathbf{s}_{1u}\times\mathbf{s}_{1v} &= \mathbf{s}_u\times\mathbf{s}_v \\ \mathbf{s}_{2u}\times\mathbf{s}_{2v} &= (1-2B\kappa_{\mathrm{M}}+B^2\kappa_{\mathrm{G}})\mathbf{s}_u\times\mathbf{s}_v \end{aligned}$$

which yields, in eq. (59):

$$\begin{aligned} &\left\langle \mathbf{s}_2-\mathbf{s}_1, \tilde{\mathbf{s}}_u\times\tilde{\mathbf{s}}_v\right\rangle \\ &= \left\langle \mathbf{s}_{[B]}-\mathbf{s}, ((1-\alpha)\mathbf{s}_u+\alpha\mathbf{s}_{[B]_u})\times((1-\alpha)\mathbf{s}_v+\alpha\mathbf{s}_{[B]_v})\right\rangle \\ &= \Big\langle B\mathbf{n} \ , \ (1-\alpha)^2\mathbf{s}_u\times\mathbf{s}_v \\ &\qquad +\alpha(1-\alpha)(\mathbf{s}_u\times\mathbf{s}_{[B]_v}+\mathbf{s}_{[B]_u}\times\mathbf{s}_v)+\alpha^2\mathbf{s}_{[B]_u}\times\mathbf{s}_{[B]_v}\Big\rangle \\ &= \Big\langle B\mathbf{n} \ , \ (1-\alpha)^2\mathbf{s}_u\times\mathbf{s}_v \\ &\qquad +\alpha(1-\alpha)(2\mathbf{s}_u\times\mathbf{s}_v+B(\mathbf{s}_u\times\mathbf{n}_v+\mathbf{n}_u\times\mathbf{s}_v)) \\ &\qquad +\alpha^2\mathbf{s}_{[B]_u}\times\mathbf{s}_{[B]_v}\Big\rangle \end{aligned}$$

Thanks to eq. (27) and (28), this reduces to:

$$\begin{aligned} &\left\langle \mathbf{s}_2-\mathbf{s}_1, \tilde{\mathbf{s}}_u\times\tilde{\mathbf{s}}_v\right\rangle \\ &= \Big\langle B\frac{\mathbf{s}_u\times\mathbf{s}_v}{\|\mathbf{s}_u\times\mathbf{s}_v\|} \ , \ (1-\alpha)^2\mathbf{s}_u\times\mathbf{s}_v \\ &\quad +\alpha(1-\alpha)(2\mathbf{s}_u\times\mathbf{s}_v-2B\mathbf{s}_u\times\mathbf{s}_v) \\ &\quad +\alpha^2(1-2B\kappa_{\mathrm{M}}+B^2\kappa_{\mathrm{G}})\mathbf{s}_u\times\mathbf{s}_v\Big\rangle \\ &= B\,\|\mathbf{s}_u\times\mathbf{s}_v\|\,(1-2\alpha B\kappa_{\mathrm{M}}+\alpha^2B^2\kappa_{\mathrm{G}}) \end{aligned}$$

which yields, for $J(f,\mathcal{B}_{\mathrm{in}})$:

$$\begin{aligned} J(f,\mathcal{B}_{\mathrm{in}}) = \iiint_{\Omega^2}\int_0^1 \Big\{ \\ Bf(\mathbf{s}+\alpha B\mathbf{n})\,\|\mathbf{s}_u\times\mathbf{s}_v\|\,(1-2\alpha B\kappa_{\mathrm{M}}+\alpha^2B^2\kappa_{\mathrm{G}})\Big\}\, d\alpha du dv \end{aligned}$$

Introducing a variable thickness $b=\alpha B$, we get the final form of $J(f,\mathcal{B}_{\mathrm{in}})$:

$$\begin{aligned} &J(f,\mathcal{B}_{\mathrm{in}}) = \\ &\iiint_{\Omega^2}\int_0^B f(\mathbf{s}+b\mathbf{n})\,\|\mathbf{s}_u\times\mathbf{s}_v\|\,(1-2b\kappa_{\mathrm{M}}+b^2\kappa_{\mathrm{G}})db du dv \end{aligned}$$

## B. Calculus of variations

In this section, we calculate the variational derivative of the region term $J(f,R_{\mathrm{in}[B]})$ with respect to contour position $\mathbf{c}$.

*B.1. Variational derivative: general expression*

We consider the general energy functional, depending on the parallel curve $\Gamma_{[B]}$

$$E = \int_\Omega \mathcal{L}(\mathbf{c}_{[B]}, \mathbf{c}_{[B]_u})du$$

As is, the variational derivative of $E$ with respect to position vector $\mathbf{c}$ is difficult to write, but it is straightforward to express it with respect to the parallel position vector $\mathbf{c}_{[B]}$:

$$\frac{\delta E}{\delta\Gamma_{[B]}} = \frac{\partial\mathcal{L}}{\partial\mathbf{c}_{[B]}} - \frac{d}{du}\left\{\frac{\partial\mathcal{L}}{\partial\mathbf{c}_{[B]_u}}\right\}$$

The purpose here is to express $\delta E/\delta\mathbf{c}$ as a function of $\delta E/\delta\mathbf{c}_{[B]}$, for a general energy term $\mathcal{L}$. To some extent, we design a chain rule for the variational derivatives of parallel curve-based energies. In what follows, a partial derivative containing vector quantities should be understood as a matrix:

$$\frac{\partial\mathbf{a}}{\partial\mathbf{b}} = \begin{bmatrix} \frac{\partial a_x}{\partial b_x} & \frac{\partial a_y}{\partial b_x} \\ \frac{\partial a_x}{\partial b_y} & \frac{\partial a_y}{\partial b_y} \end{bmatrix}$$

The partial derivative of a scalar quantity with respect to a position vector (or a derivative of this position vector) is the column vector:

$$\frac{\partial\mathcal{L}}{\partial\mathbf{c}} = \begin{bmatrix} \frac{\partial\mathcal{L}}{\partial x} & \frac{\partial\mathcal{L}}{\partial y} \end{bmatrix}^T$$

We expand the partial derivatives of $\mathcal{L}$ with the chain rule. First, we differentiate with respect to $\mathbf{c}$:

$$\frac{\partial\mathcal{L}}{\partial\mathbf{c}} = \frac{\partial\mathbf{c}_{[B]}}{\partial\mathbf{c}}\frac{\partial\mathcal{L}}{\partial\mathbf{c}_{[B]}} \qquad (60)$$

and $\mathbf{c}_u$:

$$\frac{\partial \mathcal{L}}{\partial \mathbf{c}_u} = \frac{\partial \mathbf{c}_{[B]}}{\partial \mathbf{c}_u}\frac{\partial \mathcal{L}}{\partial \mathbf{c}_{[B]}} + \frac{\partial \mathbf{c}_{[B]_u}}{\partial \mathbf{c}_u}\frac{\partial \mathcal{L}}{\partial \mathbf{c}_{[B]_u}}$$

which yields

$$\begin{aligned}\frac{d}{du}\left\{\frac{\partial \mathcal{L}}{\partial \mathbf{c}_u}\right\} = &\left(\frac{\partial \mathbf{c}_{[B]}}{\partial \mathbf{c}_u}\right)_u \frac{\partial \mathcal{L}}{\partial \mathbf{c}_{[B]}} + \frac{\partial \mathbf{c}_{[B]}}{\partial \mathbf{c}_u}\left(\frac{\partial \mathcal{L}}{\partial \mathbf{c}_{[B]}}\right)_u \\ &+ \left(\frac{\partial \mathbf{c}_{[B]_u}}{\partial \mathbf{c}_u}\right)_u \frac{\partial \mathcal{L}}{\partial \mathbf{c}_{[B]_u}} + \frac{\partial \mathbf{c}_{[B]_u}}{\partial \mathbf{c}_u}\left(\frac{\partial \mathcal{L}}{\partial \mathbf{c}_{[B]_u}}\right)_u\end{aligned} \tag{61}$$

With respect to $\mathbf{c}_{uu}$, we have:

$$\frac{\partial \mathcal{L}}{\partial \mathbf{c}_{uu}} = \frac{\partial \mathbf{c}_{[B]_u}}{\partial \mathbf{c}_{uu}}\frac{\partial \mathcal{L}}{\partial \mathbf{c}_{[B]_u}}$$

which gives:

$$\begin{aligned}\frac{d^2}{du^2}\left\{\frac{\partial \mathcal{L}}{\partial \mathbf{c}_{uu}}\right\} = &\left(\frac{\partial \mathbf{c}_{[B]_u}}{\partial \mathbf{c}_{uu}}\right)_{uu} \frac{\partial \mathcal{L}}{\partial \mathbf{c}_{[B]_u}} \\ &+ 2\left(\frac{\partial \mathbf{c}_{[B]_u}}{\partial \mathbf{c}_{uu}}\right)_u \left(\frac{\partial \mathcal{L}}{\partial \mathbf{c}_{[B]_u}}\right)_u + \frac{\partial \mathbf{c}_{[B]_u}}{\partial \mathbf{c}_{uu}}\left(\frac{\partial \mathcal{L}}{\partial \mathbf{c}_{[B]_u}}\right)_{uu}\end{aligned} \tag{62}$$

Gathering (60), (61) and (62), we obtain:

$$\begin{aligned}\frac{\delta E}{\delta \Gamma} = &\underbrace{\frac{\partial \mathcal{L}}{\partial \mathbf{c}_{[B]}} - \left(\frac{\partial \mathbf{c}_{[B]}}{\partial \mathbf{c}_u}\right)_u \frac{\partial \mathcal{L}}{\partial \mathbf{c}_{[B]}}}_{(1)} - \underbrace{\frac{\partial \mathbf{c}_{[B]}}{\partial \mathbf{c}_u}\left(\frac{\partial \mathcal{L}}{\partial \mathbf{c}_{[B]}}\right)_u}_{(2)} \\ &+ \underbrace{\left(\left(\frac{\partial \mathbf{c}_{[B]_u}}{\partial \mathbf{c}_{uu}}\right)_{uu} - \left(\frac{\partial \mathbf{c}_{[B]_u}}{\partial \mathbf{c}_u}\right)_u\right)\frac{\partial \mathcal{L}}{\partial \mathbf{c}_{[B]_u}}}_{(3)} \\ &+ \underbrace{\left(2\left(\frac{\partial \mathbf{c}_{[B]_u}}{\partial \mathbf{c}_{uu}}\right)_u - \frac{\partial \mathbf{c}_{[B]_u}}{\partial \mathbf{c}_u}\right)\left(\frac{\partial \mathcal{L}}{\partial \mathbf{c}_{[B]_u}}\right)_u}_{(4)} \\ &+ \underbrace{\frac{\partial \mathbf{c}_{[B]_u}}{\partial \mathbf{c}_{uu}}\left(\frac{\partial \mathcal{L}}{\partial \mathbf{c}_{[B]_u}}\right)_{uu}}_{(5)}\end{aligned} \tag{63}$$

All derivatives of $\mathbf{c}_{[B]}$ and $\mathbf{c}_{[B]_u}$ appearing in eq. (63) are expanded in the Frenet basis, where any vector $\mathbf{x}$ may be expressed as a combination of tangent and normal vectors:

$$\mathbf{x} = \langle \mathbf{x}, \mathbf{t} \rangle \, \mathbf{t} + \langle \mathbf{x}, \mathbf{n} \rangle \, \mathbf{n}$$

We have:

$$\frac{\partial \mathbf{c}_{[B]}}{\partial x} = [1 \quad 0]^T \qquad \frac{\partial \mathbf{c}_{[B]}}{\partial y} = [0 \quad 1]^T$$

$$\frac{\partial \mathbf{c}_{[B]}}{\partial x_u} = \frac{By_u}{\ell^2}\mathbf{t} \qquad \frac{\partial \mathbf{c}_{[B]}}{\partial y_u} = -\frac{Bx_u}{\ell^2}\mathbf{t}$$

$$\begin{aligned}\left(\frac{\partial \mathbf{c}_{[B]}}{\partial x_u}\right)_u &= B\left(\frac{x_u\kappa}{\ell} - \frac{y_u\ell_u}{\ell^3}\right)\mathbf{t} + \frac{By_u\kappa}{\ell}\mathbf{n} \\ \left(\frac{\partial \mathbf{c}_{[B]}}{\partial y_u}\right)_u &= B\left(\frac{y_u\kappa}{\ell} + \frac{x_u\ell_u}{\ell^3}\right)\mathbf{t} - \frac{Bx_u\kappa}{\ell}\mathbf{n}\end{aligned}$$

$$\begin{aligned}\frac{\partial \mathbf{c}_{[B]_u}}{\partial x_u} &= \left(\frac{x_u}{\ell} + B\left(\frac{x_u\kappa}{\ell} - \frac{y_u\ell_u}{\ell^3}\right)\right)\mathbf{t} - \frac{y_u}{\ell}(1 - B\kappa)\mathbf{n} \\ \frac{\partial \mathbf{c}_{[B]_u}}{\partial y_u} &= \left(\frac{y_u}{\ell} + B\left(\frac{y_u\kappa}{\ell} + \frac{x_u\ell_u}{\ell^3}\right)\right)\mathbf{t} + \frac{x_u}{\ell}(1 - B\kappa)\mathbf{n}\end{aligned}$$

$$\frac{\partial \mathbf{c}_{[B]_u}}{\partial x_{uu}} = \frac{By_u}{\ell^2}\mathbf{t} \qquad \frac{\partial \mathbf{c}_{[B]_u}}{\partial y_{uu}} = -\frac{Bx_u}{\ell^2}\mathbf{t}$$

$$\begin{aligned}\left(\frac{\partial \mathbf{c}_{[B]_u}}{\partial x_{uu}}\right)_u &= B\left(\frac{x_u\kappa}{\ell} - \frac{y_u\ell_u}{\ell^3}\right)\mathbf{t} + \frac{By_u\kappa}{\ell}\mathbf{n} \\ \left(\frac{\partial \mathbf{c}_{[B]_u}}{\partial y_{uu}}\right)_u &= B\left(\frac{y_u\kappa}{\ell} + \frac{x_u\ell_u}{\ell^3}\right)\mathbf{t} - \frac{Bx_u\kappa}{\ell}\mathbf{n}\end{aligned}$$

Incidentally, the following relation is verified:

$$\left(\frac{\partial \mathbf{c}_{[B]_u}}{\partial \mathbf{c}_u}\right)_u = \left(\frac{\partial \mathbf{c}_{[B]_u}}{\partial \mathbf{c}_{uu}}\right)_{uu}$$

The previous forms allow us to expand the underbraced terms in eq. (63):

$$\begin{aligned}(1) = &\frac{\partial \mathcal{L}}{\partial \mathbf{c}_{[B]}} - \frac{B\ell_u}{\ell^2}\left\langle \frac{\partial \mathcal{L}}{\partial \mathbf{c}_{[B]}}, \mathbf{t} \right\rangle \mathbf{n} \\ &- B\kappa\left\langle \frac{\partial \mathcal{L}}{\partial \mathbf{c}_{[B]}}, \mathbf{t} \right\rangle \mathbf{t} + B\kappa\left\langle \frac{\partial \mathcal{L}}{\partial \mathbf{c}_{[B]}}, \mathbf{n} \right\rangle \mathbf{n} \\ (2) = &-\frac{B}{\ell}\left\langle \left(\frac{\partial \mathcal{L}}{\partial \mathbf{c}_{[B]}}\right)_u, \mathbf{t} \right\rangle \mathbf{n} \\ (3) = &\, 0 \\ (4) = &(B\kappa - 1)\left\langle \left(\frac{\partial \mathcal{L}}{\partial \mathbf{c}_{[B]_u}}\right)_u, \mathbf{t} \right\rangle \mathbf{t} + \frac{B\ell_u}{\ell^2}\left\langle \left(\frac{\partial \mathcal{L}}{\partial \mathbf{c}_{[B]_u}}\right)_u, \mathbf{t} \right\rangle \mathbf{n} \\ &- (1 + B\kappa)\left\langle \left(\frac{\partial \mathcal{L}}{\partial \mathbf{c}_{[B]_u}}\right)_u, \mathbf{n} \right\rangle \mathbf{n} \\ (5) = &-\frac{B}{\ell}\left\langle \left(\frac{\partial \mathcal{L}}{\partial \mathbf{c}_{[B]_u}}\right)_{uu}, \mathbf{t} \right\rangle \mathbf{n}\end{aligned}$$

We factorize:

$$\begin{aligned}\frac{\delta E}{\delta \Gamma} = &(1 - B\kappa)\left\langle \frac{\partial \mathcal{L}}{\partial \mathbf{c}_{[B]}} - \left(\frac{\partial \mathcal{L}}{\partial \mathbf{c}_{[B]_u}}\right)_u, \mathbf{t} \right\rangle \mathbf{t} \\ &+ (1 + B\kappa)\left\langle \frac{\partial \mathcal{L}}{\partial \mathbf{c}_{[B]}} - \left(\frac{\partial \mathcal{L}}{\partial \mathbf{c}_{[B]_u}}\right)_u, \mathbf{n} \right\rangle \mathbf{n} \\ &- \frac{B\ell_u}{\ell^2}\left\langle \frac{\partial \mathcal{L}}{\partial \mathbf{c}_{[B]}} - \left(\frac{\partial \mathcal{L}}{\partial \mathbf{c}_{[B]_u}}\right)_u, \mathbf{t} \right\rangle \mathbf{n} \\ &+ \frac{B}{\ell}\left\langle \left(\frac{\partial \mathcal{L}}{\partial \mathbf{c}_{[B]}}\right)_u - \left(\frac{\partial \mathcal{L}}{\partial \mathbf{c}_{[B]_u}}\right)_{uu}, \mathbf{t} \right\rangle \mathbf{n}\end{aligned}$$

which is rewritten using the variational derivative of $E$ with respect to $\mathbf{c}_{[B]}$. We have the general formula, which relates the variational derivatives with respect to $\mathbf{c}$

and $\mathbf{c}_{[B]}$:

$$\frac{\delta E}{\delta \Gamma} = (1-B\kappa)\left\langle \frac{\delta E}{\delta \Gamma_{[B]}}, \mathbf{t} \right\rangle \mathbf{t} + (1+B\kappa)\left\langle \frac{\delta E}{\delta \Gamma_{[B]}}, \mathbf{n} \right\rangle \mathbf{n} - \frac{B\ell_u}{\ell^2}\left\langle \frac{\delta E}{\delta \Gamma_{[B]}}, \mathbf{t} \right\rangle \mathbf{n} + \frac{B}{\ell}\left\langle \left(\frac{\delta E}{\delta \Gamma_{[B]}}\right)_u, \mathbf{t} \right\rangle \mathbf{n} \tag{64}$$

*B.2. Variational derivative: region integral over $R_{\mathrm{in}[B]}$*

The considered energy is now the area integral of any function $f$ over the region enclosed by curve $\Gamma_{[B]}$, expressed as a line integral using Green's theorem:

$$E = J(f, R_{\mathrm{in}[B]}) = \int_\Omega {x_{[B]}}_u P(\mathbf{c}_{[B]}) + {y_{[B]}}_u Q(\mathbf{c}_{[B]}) du$$

Its variational derivative with respect to $\mathbf{c}_{[B]}$ is easily determined from eq. (40), considering $\mathbf{c}_{[B]}$ instead of $\mathbf{c}$. One may find the complete mathematical derivation in the appendix of [10].

$$\frac{\delta E}{\delta \Gamma_{[B]}} = f(\mathbf{c}_{[B]}) \begin{bmatrix} {y_{[B]}}_u \\ -{x_{[B]}}_u \end{bmatrix} = -\ell(1-B\kappa) f(\mathbf{c}_{[B]})\mathbf{n} \tag{65}$$

Expression 64 needs the derivative of (65). Using the relation $\mathbf{n}_u = -\ell\kappa\mathbf{t}$, we get:

$$\left(\frac{\delta E}{\delta \Gamma_{[B]}}\right)_u = -\frac{d}{du}\left\{\ell(1-B\kappa) f(\mathbf{c}_{[B]})\right\}\mathbf{n} + \ell^2\kappa(1-B\kappa) f(\mathbf{c}_{[B]})\mathbf{t} \tag{66}$$

We substitute eqs. (65) and (66) into 64. Since $\langle \mathbf{n}, \mathbf{t} \rangle = 0$, this reduces to:

$$\frac{\delta E}{\delta \Gamma} = (1+B\kappa)\left\langle -\ell(1-B\kappa) f(\mathbf{c}_{[B]}), \mathbf{n} \right\rangle \mathbf{n} + \frac{B}{\ell}\left\langle \frac{d}{du}\left\{-\ell(1-B\kappa) f(\mathbf{c}_{[B]})\right\}\mathbf{n} + \ell^2\kappa(1-B\kappa) f(\mathbf{c}_{[B]})\mathbf{t}\ ,\ \mathbf{t} \right\rangle \mathbf{n}$$

which eventually leads to:

$$\frac{\delta E}{\delta \Gamma} = -\ell(1-B\kappa) f(\mathbf{c}_{[B]})\mathbf{n} \tag{67}$$

## References


[1] M. Kass, A. Witkin, D. Terzopoulos, Snakes: active contour models, International Journal of Computer Vision 1 (4) (1988) 321–331.

[2] Z. Zhang, F. Braun, Fully 3D active surface models with self-inflation and self-deflation forces, in: IEEE Computer Vision and Pattern Recognition (CVPR), San Juan, Puerto Rico, 1997, pp. 85–90.

[3] J. Lachaud, A. Montanvert, Deformable meshes with automated topology changes for coarse-to-fine three-dimensional surface extraction, Medical Image Analysis 3 (2) (1999) 187–207.

[4] R. Malladi, J. Sethian, B. Vemuri, Shape modeling with front propagation: a level set approach, IEEE Transactions on Pattern Analysis and Machine Intelligence 17 (2) (1995) 158–175.

[5] D. Adalsteinsson, J. Sethian, A fast level set method for propagating interfaces, Journal of Computational Physics 118 (2) (1995) 269–277.

[6] D. Mumford, J. Shah, Optimal approximation by piecewise smooth functions and associated variational problems, Communications on Pure and Applied Mathematics 42 (5) (1989) 577–685.

[7] T. Brox, D. Cremers, On the statistical interpretation of the piecewise smooth Mumford-Shah functional, in: International Conference on Scale Space and Variational Methods in Computer Vision (SSVM), Ischia, Italy, 2007, pp. 203–213.

[8] R. Ronfard, Region based strategies for active contour models, International Journal of Computer Vision 13 (2) (1994) 229–251.

[9] J. Ivins, J. Porrill, Active region models for segmenting textures and colours, Image and Vision Computing 13 (5) (1995) 431–438.

[10] S. Zhu, A. Yuille, Region competition: unifying snakes, region growing, Bayes/MDL for multiband image segmentation, IEEE Transactions on Pattern Analysis and Machine Intelligence 18 (9) (1996) 884–900.

[11] T. Chan, L. Vese, Active contours without edges, IEEE Transactions on Image Processing 10 (2) (2001) 266–277.

[12] S. Jehan-Besson, M. Barlaud, G. Aubert, DREAM$^2$S: Deformable regions driven by an eulerian accurate minimization method for image and video segmentation, International Journal of Computer Vision 53 (1) (2003) 45–70.

[13] N. Paragios, R. Deriche, Geodesic active regions and level set methods for motion estimation and tracking, Computer Vision and Image Understanding 97 (3) (2005) 259–282.

[14] G. Slabaugh, G. Unal, Active polyhedron: surface evolution theory applied to deformable meshes, in: IEEE Computer Vision and Pattern Recognition (CVPR), Vol. 2, San Diego, USA, 2005, pp. 84–91.

[15] A. Dufour, V. Shinin, S. Tajbakhsh, N. Guillén-Aghion, J.-C. Olivo-Marin, C. Zimmer, Segmenting and tracking fluorescent cells in dynamic 3-D microscopy with coupled active surfaces, IEEE Transactions on Image Processing 14 (9) (2005) 1396–1410.

[16] M. Taron, N. Paragios, M.-P. Jolly, Registration with uncertainties and statistical modeling of shapes with variable metric kernels, IEEE Transactions on Pattern Analysis and Machine Intelligence 31 (1) (2009) 99–113.

[17] N. Paragios, R. Deriche, Geodesic active regions and level set methods for supervised texture segmentation, International Journal of Computer Vision 46 (3) (2002) 223–247.

[18] J. Piovano, T. Papadopoulo, Local statistic based region segmentation with automatic scale selection, in: European Conference on Computer Vision (ECCV), Vol. 5303 of LNCS, Springer, Marseille, France, 2008, pp. 486–499.

[19] M. Alemán-Flores, L. Alvarez, V. Caselles, Texture-oriented anisotropic filtering and geodesic active contours in breast tumor ultrasound segmentation, Journal of Mathematical Imaging and Vision 28 (1) (2007) 81–97.

[20] C. Li, C. Kao, J. Gore, Z. Ding, Implicit active contours driven by local binary fitting energy, in: IEEE Computer Vision and Pattern Recognition (CVPR), Minneapolis, Minnesota, USA, 2007, pp. 17–22.

[21] S. Lankton, A. Tannenbaum, Localizing region-based active contours, IEEE Transactions on Image Processing 17 (11) (2008) 2029–2039.

[22] M. Jacob, T. Blu, M. Unser, Efficient energies and algorithms for parametric snakes, IEEE Transactions on Image Processing 13 (9) (2004) 1231–1244.

[23] R. Kimmel, Fast edge integration, S. Osher and N. Paragios (Eds), Springer-Verlag, 2003, Ch. invited chapter in Geometric Level Set Methods in Imaging, Vision and Graphics.

[24] R. Goldenberg, R. Kimmel, M. Rivlin, E. an Rudzsky, Fast geodesic active contours, IEEE Transactions on Image Processing 10 (10) (2001) 1467–1475.

[25] C. Sagiv, N. Sochen, Y. Zeevi, Integrated active contours for

texture segmentation, IEEE Transactions on Image Processing 15 (6) (2006) 1633–1646.
[26] J. Mille, R. Boné, P. Makris, H. Cardot, 2D and 3D deformable models with narrow band region energy, in: IEEE International Conference on Image Processing (ICIP), San Antonio, USA, 2007, pp. 57–60.
[27] R. Farouki, C. Neff, Analytic properties of plane offset curves, Computer Aided Geometric Design 7 (1-4) (1990) 83–99.
[28] A. Gray, Modern differential geometry of curves and surfaces with Mathematica, CRC Press, $2^{nd}$ edition, 1997.
[29] V. Caselles, R. Kimmel, G. Sapiro, Geodesic active contours, International Journal of Computer Vision 22 (1) (1997) 61–79.
[30] S. Kichenassamy, A. Kumar, A. Olver, P.and Tannenbaum, A. Yezzi, Gradient flows and geometric active contour models, in: IEEE International Conference on Computer Vision (ICCV), Boston, MA, USA, 1995, pp. 810–815.
[31] B. Appleton, H. Talbot, Globally optimal geodesic active contours, Journal of Mathematical Imaging and Vision 23 (1) (2005) 67–86.
[32] G. Elber, L. In-Kwon, K. Myung-Soo, Comparing offset curve approximation methods, IEEE Computer Graphics and Applications 17 (3) (1997) 62–71.
[33] A. Pressley, Elementary differential geometry, Springer, 2002.
[34] M. do Carmo, Differential geometry of curves and surfaces, Prentice-Hall, 1976.
[35] L. Cohen, I. Cohen, Finite element methods for active contour models and balloons for 2D and 3D images, IEEE Transactions on Pattern Analysis and Machine Intelligence 15 (11) (1993) 1131–1147.
[36] R. Goldenberg, R. Kimmel, M. Rivlin, E. an Rudzsky, Cortex segmentation: a fast variational geometric approach, IEEE Transactions on Medical Imaging 21 (2) (2002) 1544–1551.
[37] T. McInerney, D. Terzopoulos, A dynamic finite element surface model for segmentation and tracking in multidimensional medical images with application to cardiac 4D image analysis, Computerized Medical Imaging and Graphics 19 (1) (1995) 69–83.
[38] M. Desbrun, M. Meyer, P. Schröder, A. Barr, Implicit fairing of irregular meshes using diffusion and curvature flow, in: $26^{th}$ ACM Conference on Computer Graphics and Interactive Techniques (SIGGRAPH), Los Angeles, USA, 1999, pp. 317–324.
[39] M. Meyer, M. Desbrun, P. Schröder, A. Barr, Discrete differential geometry operators for triangulated 2-manifolds, in: International Workshop on Visualization and Mathematics (VisMath), Berlin-Dahlem , Germany, 2002, pp. 35–57.
[40] G. Charpiat, P. Maurel, J.-P. Pons, R. Keriven, O. Faugeras, Generalized gradients: priors on minimization flows, International Journal of Computer Vision 73 (3) (2007) 325–344.
[41] J. Oliensis, Local reproducible smoothing without shrinkage, IEEE Transactions on Pattern Analysis and Machine Intelligence 15 (3) (1993) 307–312.
[42] G. Taubin, Curve and surface smoothing without shrinkage, in: IEEE International Conference on Computer Vision (ICCV), Boston, MA, USA, 1995, pp. 852–957.
[43] L. Staib, A. Chakraborty, J. Duncan, An integrated approach for locating neuroanatomical structure from MRI, International Journal of Pattern Recognition and Artificial Intelligence 11 (8) (1997) 1247–1269.
[44] Y. Shi, W. Karl, Real-time tracking using level sets, in: IEEE Computer Vision and Pattern Recognition (CVPR), Vol. 2, San Diego, USA, 2005, pp. 34–41.
[45] G. Chung, L. Vese, Energy minimization based segmentation and denoising using a multilayer level set approach, in: $5^{th}$ International Workshop on Energy Minimization Methods in Computer Vision and Pattern Recognition (EMMCVPR), Vol. 3757 of LNCS, Springer, St. Augustine, FL, USA, 2005, pp. 439–455.
[46] C. Le Guyader, L. Vese, Self-repelling snakes for topology-preserving segmentation models, IEEE Transactions on Image Processing 17 (5) (2008) 767–779.
[47] X. Zeng, L. Staib, R. Schultz, J. Duncan, Segmentation and measurement of the cortex from 3D MR images using coupled surfaces propagation, IEEE Transactions on Medical Imaging 18 (10) (1999) 927–937.
[48] J. Ivins, J. Porrill, Constrained active region models for fast tracking in color image sequences, Computer Vision and Image Understanding 72 (1) (1998) 54–71.
[49] A. Mansouri, A. Mitiche, C. Vazquez, Multiregion competition: a level set extension of region competition to multiple region image partitioning, Computer Vision and Image Understanding 101 (3) (2006) 137–150.
[50] L. Pi, C. Shen, F. Li, J. Fan, A variational formulation for segmenting desired objects in color images, Image and Vision Computing 25 (9) (2007) 1414–1421.
[51] J. Mille, R. Boné, L. Cohen, Region-based 2D deformable generalized cylinder for narrow structures segmentation, in: European Conference on Computer Vision (ECCV), Vol. 5303 of LNCS, Springer, Marseille, France, 2008, pp. 392–404.